High-resolution Fourier-transform spectroscopy and deperturbation analysis of the A1(v = 1) level in 12C18O

Malicka, M. I.; Ryzner, S.; Heays, A. N.; de Oliveira, N.; Field, R. W.; Ubachs, W.; Hakalla, R.

published in
Journal of Quantitative Spectroscopy and Radiative Transfer
2020

DOI (link to publisher)
10.1016/j.jqsrt.2020.107243

document version
Publisher's PDF, also known as Version of record

document license
Article 25fa Dutch Copyright Act

Journal of Quantitative Spectroscopy & Radiative Transfer 255 (2020) 107243

Contents lists available at ScienceDirect

Journal of Quantitative Spectroscopy & Radiative Transfer

journal homepage: www.elsevier.com/locate/jqsrt

High-resolution Fourier-transform spectroscopy and deperturbation analysis of the $A^1\Pi(v = 1)$ level in $^{12}C^{18}O$

M.I. Malicka[a], S. Ryzner[b], A.N. Heays[c,d], N. de Oliveira[e], R.W. Field[f], W. Ubachs[g], R. Hakalla[b,*]

[a] The Faculty of Mathematics and Applied Physics, Rzeszów University of Technology, Powstańców Warszawy 8 Street, 35-959 Rzeszów, Poland
[b] Materials Spectroscopy Laboratory, Institute of Physics, University of Rzeszów, Pigonia 1 Street, 35-310 Rzeszów, Poland
[c] School of Earth and Space Exploration, Arizona State University, Tempe, AZ85281, United States
[d] NASA Astrobiology Institute, NASA Ames Research Center, Moffett Field, California, United States
[e] Synchrotron SOLEIL, Orme de Merisiers, St. Aubin, BP 48, F-91192 Gif sur Yvette Cedex, France
[f] Department of Chemistry, Massachusetts Institute of Technology, Cambridge, MA02139, United States
[g] Department of Physics and Astronomy, and LaserLaB, Vrije Universiteit, De Boelelaan 1081, 1081HV Amsterdam, the Netherlands

ARTICLE INFO

Article history:
Received 14 April 2020
Revised 15 July 2020
Accepted 3 August 2020
Available online 4 August 2020

Keywords:
Fourier-transform spectroscopy
High-resolution VUV and VIS spectra
Deperturbation analysis
Spin-orbit spin-electronic and rotation-electronic couplings
CO
Isotopologues

ABSTRACT

The $A^1\Pi(v = 1)$ level of the $^{12}C^{18}O$ isotopologue was precisely reinvestigated with two complementary spectroscopic techniques. High resolution $B^1\Sigma^+ \rightarrow A^1\Pi(0, 1)$, (1, 1) and $C^1\Sigma^+ \rightarrow A^1\Pi(0, 1)$ emission bands were recorded in the visible region, 20,700 – 26,100 cm^{-1}, with a 1.71 m Fourier-transform spectrometer (Bruker IFS 125-HR) installed at the University of Rzeszów. The resulting line centre accuracy of isolated and medium to strong lines is 0.005 cm^{-1}. In addition, high-resolution spectra of the $A^1\Pi \longleftarrow X^1\Sigma^+(1, 0)$, $B^1\Sigma^+ \longleftarrow X^1\Sigma^+(0, 0)$ and (1, 0) as well as $C^1\Sigma^+ \longleftarrow X^1\Sigma^+(0, 0)$ bands were recorded between 66,200 and 95,250 cm^{-1} using the vacuum-ultraviolet Fourier-transform spectrometer installed at the DESIRS beamline of the SOLEIL synchrotron. The wavenumber accuracy for isolated and strong spectral lines is 0.01 cm^{-1}. A data set of 626 spectral lines belonging to seven bands was incorporated into a global deperturbation analysis. Significantly improved deperturbed molecular constants for the $A^1\Pi(v = 1)$, $a'^3\Sigma^+(v = 10)$, $D^1\Delta(v = 1)$, and $I^1\Sigma^-(v = 2)$ levels, term values of the $B^1\Sigma^+(v = 0, 1)$ and $C^1\Sigma^+(v = 0)$ Rydberg states as well as the accompanying spin-orbit and rotation-electronic (***L***-uncoupling) interaction parameters were obtained. The experimental ro-vibrational term values of the $A^1\Pi(v = 1)$ level and its perturbers were also determined. The mixed composition of interacting states is expressed in terms of their $^1\Pi$ percentage character.

1. Introduction

The spectroscopy of the carbon monoxide molecule is of major astrophysical significance because it is the second most abundant chemical compound in the interstellar medium (ISM), after molecular hydrogen, and influences chemical dynamics there through its photolysis by vacuum-ultraviolet stellar radiation [1]. The detection of CO and determination of its local density and temperature are essential for modelling the beginning of stellar evolution, the dynamics of interstellar clouds and nebulae, the atmospheres of planets and exoplanets, the characterisation of extra-galactic clouds, and the search for varying fundamental constants in the early Universe [2–7]. CO isotopologues are often probed as proxies for the hydrogen content of molecular clouds and map the distribution of matter therein [8–10]. Quantitative detections of multiple CO isotopologues can solve for the "depth effect" in interstellar absorption and be used to determine $[^{12}C]/[^{13}C]$ and $[^{16}O]/[^{17}O]/[^{18}O]$ ratios in the ISM [11–13]. All natural isotopologues, including $^{12}C^{18}O$, have been found, inter alia, in high-resolution Solar spectra [14], interstellar clouds [2,8,9] and nebulae [2].

From a pure molecular physics perspective, the $A^1\Pi$ electronic state of CO is a show-case example of complex multi-level perturbative structure with associated breakdown of the Born-Oppenheimer approximation [15–17]. The $A^1\Pi$ state of $^{12}C^{18}O$ was previously studied via the Ångström system ($B^1\Sigma^+ - A^1\Pi$) by Rytel [18], Janjić et al. [19], Kępa [20], Kępa et al. [21] and Trivikram et al. [22]; the Herzberg system ($C^1\Sigma^+ - A^1\Pi$) by Kępa [23] and

* Corresponding author.
E-mail address: hakalla@ur.edu.pl (R. Hakalla).

https://doi.org/10.1016/j.jqsrt.2020.107243
0022-4073/

Janjić et al. [24]; and the Kępa-Rytel system ($E^1\Pi$ – $A^1\Pi$) by Kępa et al. [25] and Kępa [20]. The other band systems investigated for the $^{12}C^{18}O$ isotopologue are: 4th Positive ($A^1\Pi$ – $X^1\Sigma^+$) [22,26–29]; Hopfield-Birge ($B^1\Sigma^+$ – $X^1\Sigma^+$) [22,27,30–33], $C^1\Sigma^+$ – $X^1\Sigma^+$ [27,31–35], $E^1\Pi$– $X^1\Sigma^+$ [26,31–33,36], and $C^1\Sigma^+$ – $B^1\Sigma^+$[37].

A deperturbation analysis of the $A^1\Pi$ state of CO was first made by Field and co-workers in the early 1970's [38,39]. They analysed the $v = 0$ – 23 vibrational levels on the basis of experimental A – X bands measured by classical spectroscopy to an accuracy of 0.1 cm^{-1}. Recently, the $A^1\Pi$ electronic state in $^{12}C^{16}O$ was accurately re-examined using two experimental techniques: two-photon Doppler-free laser spectroscopy with 0.002 cm^{-1} accuracy and synchrotron based Fourier-transform (VUV-FT) spectroscopy with an accuracy as good as 0.01 cm^{-1} [40,41]. Deperturbation analyses of the $A^1\Pi$ state in other isotopologues have been conducted as well: Niu et al. [42] for $^{13}C^{16}O$ A($v = 0$), Hakalla et al. [43] for $^{12}C^{17}O$ A($v = 1$ – 5), Hakalla et al. [44] for $^{13}C^{17}O$ A($v = 0$ – 3) and Hakalla et al. [45] for $^{13}C^{18}O$ A($v = 0$). These analyses were carried out on the basis of experimental spectra obtained by three complementary techniques: FT emission spectroscopy in the VIS range with an accuracy of about 0.005 cm^{-1}, VUV-FT absorption spectroscopy based on synchrotron radiation with accuracy of about 0.02 cm^{-1} and two-photon Doppler-free laser spectroscopy with accuracy up to 0.003 cm^{-1}. Previous deperturbation analyses of $A^1\Pi$ levels in $^{12}C^{18}O$, the isotopologue of present interest, were carried out by Haridass et al. [26] for the $v = 1$ and 2 vibrational levels based on A – X bands obtained with a 10.6 m vacuum grating spectrograph to an accuracy of 0.1 cm^{-1}; Beaty et al. [28] for the A($v = 0$ – 9) levels based on the A – X spectra with accuracy of 0.2 cm^{-1} recorded in a supersonic jet expansion experiment; and Trivikram et al. [22] for the A($v = 0$) level with an accuracy of 0.001 – 0.005 cm^{-1} using the three complementary techniques mentioned above. Thus, while a highly accurate deperturbation analysis exists for A($v = 0$) in $^{12}C^{18}O$ [22], this class of analysis has not been made for higher vibrational levels.

The goal of the present study is to perform a new highly-accurate deperturbation analysis of the $A^1\Pi(v = 1)$ level of $^{12}C^{18}O$ in a continuation of high-precision analyses of the perturbed level structure of the $A^1\Pi$ state for all carbon monoxide isotopologues. This work is based on high-quality spectra obtained by two complementary experimental techniques: FT emission spectroscopy in the VIS range from a hollow-cathode tube and VUV-FT absorption spectroscopy with synchrotron radiation.

2. Experimental details and measurements

2.1. VIS-FT spectroscopy (University of Rzeszów)

An analysis of the $B^1\Sigma^+ \rightarrow A^1\Pi$ (0, 1), (1, 1) and $C^1\Sigma^+ \rightarrow A^1\Pi$ (0, 1) bands in their respective spectral regions, 20,700 – 21,400 cm^{-1}, 22,700 – 23,000 cm^{-1}, and 25,700 – 26,100 cm^{-1}, was conducted based on a spectrum obtained during a previous study described in Ref. [22]. Here, we provide some brief information about the experimental conditions. The emission spectrum of the $^{12}C^{18}O$ bands was obtained using an air-cooled carbon hollow-cathode lamp filled with isotopically enriched molecular oxygen (Sigma-Aldrich, 98.1% of $^{18}O_2$) to a pressure of 3 mbar. A 54 mA electric current flowed through the gas with a 780 V DC voltage applied to the electrodes.

The rotational temperature of intra-cathode plasma was determined to be 1100(50) K, and allowed for the recording of transitions associated with rotational levels as high as $J = 40$, 22 and 31 for the B – A(0, 1), B – A(1, 1), and C – A(0, 1) bands, respectively. This resulted in greater spectral line Doppler-broadening (to 0.1 cm^{-1} full-width-at-half-maximum, FWHM) than in some of our previous studies where the plasma temperature was only

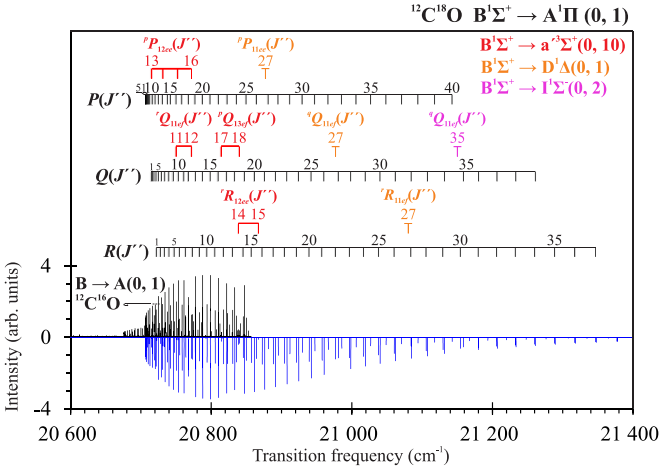

Fig. 1. High-resolution emission spectrum of the $^{12}C^{18}O$ $B^1\Sigma^+$- $A^1\Pi$(0, 1) band as well as the $^{12}C^{18}O$ $B^1\Sigma^+$ - $a'^3\Sigma^+$(0, 10), $B^1\Sigma^+$ - $D^1\Delta$(0, 1) and $B^1\Sigma^+$ - $I^1\Sigma^-$(0, 2) extra-lines recorded with the VIS-FT spectrometer. Upper trace: experimental spectrum; the $^{12}C^{16}O$ $B^1\Sigma^+$ - $A^1\Pi$(0, 1) transitions were treated as contamination during the analysis. Lower trace: simulation of the $^{12}C^{18}O$ $B^1\Sigma^+$ - $A^1\Pi$(0, 1) band together with the $^{12}C^{18}O$ $B^1\Sigma^+$ - $a'^3\Sigma^+$(0, 10), $B^1\Sigma^+$ - $D^1\Delta$(0, 1) and $B^1\Sigma^+$ - $I^1\Sigma^-$(0, 2) extra-lines, obtained with the PGOPHER software [50,51].

about 300 K [46–48]. Spectra of $^{12}C^{18}O$ were obtained by coupling the emission from the hollow-cathode region unto a 1.71 m Bruker spectrometer (IFS 125-HR) working under vacuum conditions, and installed at the University of Rzeszów [42,49]. The final spectrum was produced after acquiring 128 FT-scans conducted with an instrumental resolution of 0.018 cm^{-1}. The signal-to-noise ratios (SNR), achieved for the B – A(0, 1), C – A(0, 1) and B – A(1, 1) bands were 80 : 1, 10 : 1 and 8 : 1, respectively. The spectra are contaminated by lines of $^{12}C^{16}O$ as a result of a small $^{16}O_2$ impurity in the gas mixture.

Calibration of the frequency axis was carried out using the He-Ne line (633 nm) from an FT internally-stabilised laser source, resulting in an accuracy of 0.004 cm^{-1} (1σ). The centre frequencies of spectral lines were determined by fitting Voigt profiles to the experimental spectrum. This resulted in estimated line frequency accuracies of 0.005, 0.008 and 0.01 cm^{-1} for isolated medium to strong lines in the B – A(0, 1), B – A(1, 1) and C – A(0, 1) bands, respectively, and poorer respective accuracies of 0.02, 0.03 and 0.04 cm^{-1} for weak and/or blended lines. Figs. 1–3 show high-resolution spectra of these bands along with rotational assignments and simulations obtained using the PGOPHER software [50,51]. Measured transition frequencies of the $^{12}C^{18}O$ B – A(0, 1), B – A(1, 1), and C – A(0, 1) bands are listed in Tables 1–3, while the frequencies of extra emission lines from $B^1\Sigma^+(v = 0)$, $B^1\Sigma^+(v = 1)$ and $C^1\Sigma^+(v = 0)$ to levels perturbing $A^1\Pi(v = 1)$ are presented in Table 4.

2.2. VUV-FT spectroscopy (SOLEIL synchrotron)

Vacuum-ultraviolet spectra containing the $A^1\Pi(v = 1) \longleftarrow X^1\Sigma^+(v = 0)$, $B^1\Sigma^+(v = 0, 1) \longleftarrow X^1\Sigma^+(v = 0)$, and $C^1\Sigma^+(v = 0) \longleftarrow X^1\Sigma^+(v = 0)$ photoabsorption bands of $^{12}C^{18}O$ were recorded on the DESIRS beamline at the SOLEIL synchrotron. Details of the beamline, spectrometer, and high-temperature absorption cell used to collect the present data, and its reduction to accurate line frequencies are given previously [22,45,52–54]. Briefly, synchrotron radiation is generated by an undulator insertion device with approximately 5 nm spectral bandwidth. A 9 cm-long MgF_2-windowed cell could be inserted onto the incident beam and filled with $^{12}C^{18}O$ (contaminated with approximately 1% $^{12}C^{16}O$, 0.4% $^{12}C^{17}O$, and 0.1% $^{13}C^{16}O$). MgF_2 is transparent in the VUV down to

Table 1
Transition frequencies of the $^{12}C^{18}O$ $B^1\Sigma^+$ – $A^1\Pi(0, 1)$ emission band obtained in the VIS-FT experiment.[a]

J''	R(J'')	o-c	Q(J'')	o-c	P(J'')	o-c
1	20,722.67(2)[b]	-0.01	20,715.244(6)	-0.005	20,711.53(1)[b]	-0.01
2	20,727.782(6)	-0.005	20,716.652(5)	-0.005	20,709.231(7)[b]	-0.004
3	20,733.605(5)	-0.002	20,718.766(5)[b]	-0.002	20,707.635(5)	-0.001
4	20,740.129(5)	-0.003	20,721.579(5)	-0.003	20,706.737(6)[b]	-0.003
5	20,747.355(5)	-0.003	20,725.100(5)[b]	-0.002	20,706.545(5)[b]	-0.003
6	20,755.286(5)	-0.001	20,729.322(5)	-0.003	20,707.058(5)	-0.003
7	20,763.916(5)	-0.003	20,734.250(5)[b]	-0.004	20,708.275(5)	-0.002
8	20,773.250(5)	-0.003	20,739.886(4)	-0.003	20,710.197(5)	-0.002
9	20,783.287(5)	-0.003	20,746.235(4)	-0.004	20,712.826(5)	-0.002
10	20,794.031(5)[b]	-0.004	20,753.319(5)[b]	-0.004	20,716.165(5)[b]	-0.002
11	20,805.488(5)	-0.006	20,761.246(4)	-0.004	20,720.223(5)	-0.001
12	20,817.699(5)	-0.008	20,767.691(5)[b]	0.006	20,725.025(5)[b]	0.001
13	20,830.744(5)	-0.001	20,778.046(4)	-0.005	20,730.657(5)	-0.004
14	20,845.408(5)	0.006	20,788.033(5)	0.001	20,737.939(5)	0.002
15	20,856.985(5)	-0.007	20,798.628(5)[b]	0.001	20,742.134(5)	-0.007
16	20,872.372(5)	-0.009	20,809.941(5)	0.003	20,750.137(5)[b]	-0.003
17	20,888.111(5)	0.003	20,822.193(5)[b]	0.008	20,758.494(5)	-0.003
18	20,904.467(5)	-0.001	20,833.56(1)	-0.02	20,767.477(5)[b]	-0.007
19	20,921.493(5)	-0.002	20,847.338(4)	-0.005	20,777.133(5)	0.005
20	20,939.201(5)	-0.002	20,861.443(4)	-0.005	20,787.476(5)[b]	0.000
21	20,957.599(5)	-0.002	20,876.193(5)	-0.003	20,798.519(5)[b]	0.001
22	20,976.694(5)[b]	-0.003	20,891.626(4)	-0.003	20,810.260(5)	0.001
23	20,996.488(5)	-0.002	20,907.758(5)	-0.003	20,822.705(5)	-0.001
24	21,016.977(5)	-0.003	20,924.595(5)	-0.002	20,835.864(5)	0.001
25	21,038.183(6)[b]	-0.002	20,942.143(4)[b]	-0.001	20,849.742(5)	0.001
26	21,060.147(5)	-0.002	20,960.453(5)	-0.002	20,864.381(5)	0.001
27	21,084.141(9)[b]	-0.001	20,980.792(5)	-0.001	20,881.063(7)[b]	0.002
28	21,105.577(5)	-0.006	20,998.596(5)	-0.001	20,895.190(5)	-0.002
29	21,129.660(6)	0.003	21,019.041(5)	0.001	20,911.961(5)	0.001
30	21,154.351(6)	-0.003	21,040.122(5)	-0.002	20,929.377(5)	0.002
31	21,179.736(9)[b]	-0.003	21,061.895(6)[b]	0.000	20,947.481(5)	-0.002
32	21,205.808(7)	-0.006	21,084.393(5)	-0.001	20,966.285(8)[b]	0.001
33	21,232.56(2)[b]	-0.01	21,107.642(5)	0.003	20,985.805(9)[b]	0.004
34	21,260.09(2)[b]	0.02	21,131.751(8)[b]	0.003	21,006.023(6)	-0.001
35	21,288.25(2)	-0.01	21,158.65(2)[b]	0.01	21,026.94(2)[b]	-0.01
36	21,317.14(2)[b]	-0.01	21,180.26(1)	0.01	21,048.618(8)	-0.005
37	21,346.73(2)	-0.01	21,206.630(7)	0.001	21,071.00(2)[b]	0.01
38	-		21,233.451(7)	0.006	21,094.092(9)	-0.002
39	-		21,260.93(1)	0.01	21,117.92(2)	-0.01
40	-		-		21,142.57(2)[w]	0.01

[a] In units of cm^{-1}. The instrumental resolution was 0.018 cm^{-1}. The uncertainties in parentheses indicate 1σ standard deviations being combinations of the random (fitting) and systematic (calibration) errors. The estimated absolute calibration uncertainty was 0.004 cm^{-1}. The absolute accuracy of the line frequency measurements was estimated to be 0.005 – 0.02 cm^{-1} depending on the line intensity and blending.

[b] Lines marked with *b* and/or *w* are blended and/or weak.

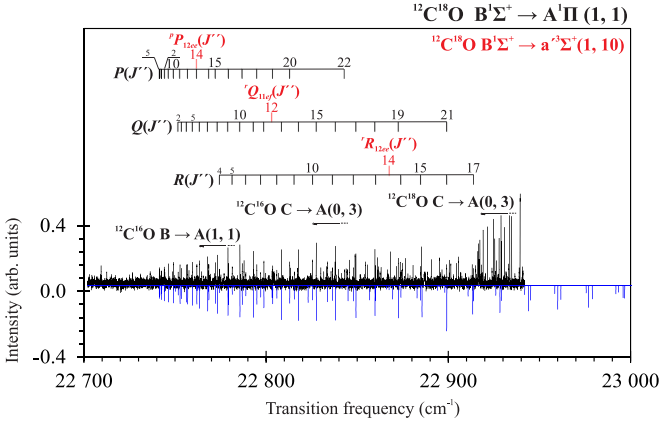

Fig. 2. High-resolution emission spectrum of the $^{12}C^{18}O$ $B^1\Sigma^+$ - $A^1\Pi(1, 1)$ band as well as the $^{12}C^{18}O$ $B^1\Sigma^+$ - $a'^3\Sigma^+(1, 10)$ extra-lines recorded with the VIS-FT spectrometer. Upper trace: experimental spectrum; the $^{12}C^{16}O$ $B^1\Sigma^+$ - $A^1\Pi(1, 1)$, $C^1\Sigma^+$ - $A^1\Pi(0, 3)$ and $^{12}C^{18}O$ $C^1\Sigma^+$ - $A^1\Pi(0, 3)$ bands were treated as contamination during the analysis. Lower trace: simulation of the $^{12}C^{18}O$ $B^1\Sigma^+$ - $A^1\Pi(1, 1)$ band together with the $^{12}C^{18}O$ $B^1\Sigma^+$ - $a'^3\Sigma^+(1, 10)$ extra-lines, obtained with the PGOPHER software [50,51].

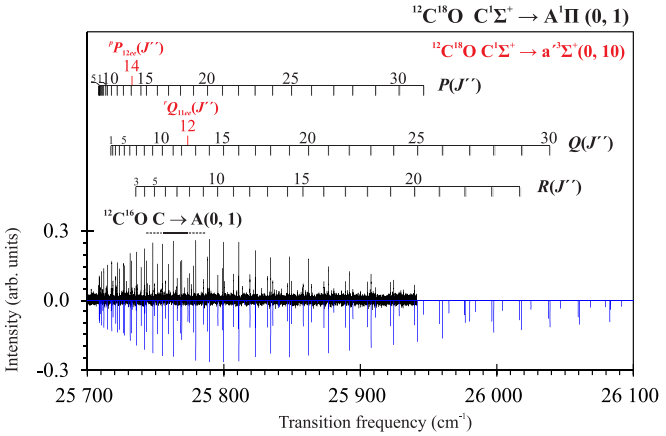

Fig. 3. High-resolution emission spectrum of the $^{12}C^{18}O$ $C^1\Sigma^+$ - $A^1\Pi(0, 1)$ band as well as the $^{12}C^{18}O$ $C^1\Sigma^+$ - $a'^3\Sigma^+(0, 10)$ extra-lines recorded with the VIS-FT spectrometer. Upper trace: experimental spectrum; the $^{12}C^{16}O$ $C^1\Sigma^+$ - $A^1\Pi(0, 1)$ band was treated as contamination during the analysis. Lower trace: simulation of the $^{12}C^{18}O$ $C^1\Sigma^+$ - $A^1\Pi(0, 1)$ band together with the $^{12}C^{18}O$ $C^1\Sigma^+$ - $a'^3\Sigma^+(0, 10)$ extra-lines, obtained with the PGOPHER software [50,51].

Table 2
Transition frequencies of the $^{12}C^{18}O$ $B^1\Sigma^+$ – $A^1\Pi(1, 1)$ emission band obtained in the VIS-FT experiment.[a]

J''	*R(J'')*	*o-c*	*Q(J'')*	*o-c*	*P(J'')*	*o-c*
1	-		-		-	
2	-		22,750.01(3)[w]	-0.01	22,742.71(4)[w b]	0.01
3	-		22,751.97(3)[b]	-0.03	22,740.99(2)[w]	-0.02
4	22,772.90(3)[w b]	-0.02	22,754.59(3)[b]	-0.02	22,739.93(3)[w b]	-0.03
5	22,779.87(3)[w b]	0.01	22,757.87(2)[b]	-0.02	22,739.58(2)[w]	0.01
6	22,787.44(3)[w]	-0.01	22,761.81(1)	-0.02	22,739.86(3)[w b]	0.02
7	22,795.69(4)[w b]	0.01	22,766.40(1)	-0.02	22,740.77(2)[w]	-0.01
8	22,804.57(2)[w]	-0.01	22,771.646(9)	-0.009	22,742.36(5)[w b]	-0.01
9	22,814.12(4)[w b]	-0.02	22,777.558(7)	-0.007	22,744.59(2)	-0.01
10	22,824.32(3)[b]	-0.03	22,784.162(7)	-0.004	22,747.48(1)	-0.01
11	22,835.21(2)	-0.02	22,791.54(1)	-0.02	22,751.06(2)	-0.01
12	22,846.77(2)	-0.02	22,797.42(1)	0.01	22,755.33(2)	-0.01
13	22,859.14(2)	-0.01	22,807.133(7)	0.003	22,760.38(3)[b]	-0.02
14	22,873.07(4)[w]	-0.01	22,816.429(8)	-0.002	22,767.04(2)[b]	0.03
15	22,883.87(2)	-0.02	22,826.29(2)[b]	-0.01	22,770.53(2)	-0.02
16	22,898.40(3)[b]	-0.04	22,836.82(2)[b]	-0.01	22,777.80(1)	-0.02
17	22,913.28(2)	-0.01	22,848.236(8)	0.001	22,785.38(2)	-0.01
18	-		22,858.73(1)	-0.02	22,793.53(2)	-0.01
19	-		22,871.57(1)	-0.02	22,802.30(2)	0.01
20	-		-		22,811.71(2)	-0.01
21	-		22,898.40(2)[b]	-0.03	-	
22	-		-		22,832.49(3)[w b]	0.01

[a] In units of cm^{-1}. The instrumental resolution was 0.018 cm^{-1}. The uncertainties in parentheses indicate 1σ standard deviations being combinations of the random (fitting) and systematic (calibration) errors. The estimated absolute calibration uncertainty was 0.004 cm^{-1}. The absolute accuracy of the line frequency measurements was estimated to be 0.008 – 0.03 cm^{-1} depending on the line intensity and blending.
[b] Lines marked with *b* and/or *w* are blended and/or weak.

Table 3
Transition frequencies of the $^{12}C^{18}O$ $C^1\Sigma^+$ – $A^1\Pi(0, 1)$ emission band obtained in the VIS-FT experiment.[a]

J''	*R(J'')*	*o-c*	*Q(J'')*	*o-c*	*P(J'')*	*o-c*
1	-		25,717.38(2)[w]	-0.01	25,713.66(4)[w b]	-0.03
2	-		25,718.78(4)[w b]	-0.01	25,711.35(3)[w]	-0.03
3	25,735.67(2)[w]	-0.01	25,720.84(2)[b]	-0.03	25,709.75(5)[w b]	-0.02
4	25,742.14(2)[w]	-0.02	25,723.63(2)	-0.02	25,708.82(3)[b]	-0.02
5	25,749.33(4)[w b]	-0.02	25,727.12(1)	-0.01	25,708.60(2)	-0.01
6	25,757.20(2)	-0.01	25,731.30(2)[b]	-0.01	25,709.08(2)	-0.01
7	25,765.77(3)[b]	-0.01	25,736.167(7)	-0.006	25,710.25(1)	-0.01
8	25,775.05(2)[b]	0.01	25,741.739(7)	-0.007	25,712.112(9)	-0.007
9	25,785.01(2)[b]	0.01	25,748.02(2)[b]	-0.01	25,714.68(2)[b]	-0.01
10	25,795.65(2)[b]	-0.01	25,755.02(1)[b]	-0.02	25,717.951(8)	-0.006
11	25,807.04(2)	0.01	25,762.869(6)	-0.007	25,721.927(8)	-0.007
12	25,819.11(2)[b]	-0.03	25,769.232(9)	0.007	25,726.649(9)	-0.001
13	25,832.06(2)	0.01	25,779.49(1)[b]	0.01	25,732.19(1)	-0.01
14	25,846.62(2)[w]	0.02	25,789.348(6)	-0.004	25,739.37(3)[b]	0.01
15	25,858.07(2)[w]	-0.02	25,799.833(6)	-0.002	25,743.450(9)	-0.009
16	25,873.33(2)	-0.01	25,811.03(1)[b]	0.01	25,751.33(1)	-0.02
17	25,888.95(2)[w]	0.01	25,823.152(7)	0.005	25,759.58(1)	-0.01
18	25,905.14(3)[w b]	-0.02	25,834.39(1)	-0.02	25,768.436(9)	-0.009
19	25,922.03(2)[w]	-0.01	25,848.024(8)	-0.006	25,777.96(1)	0.01
20	25,939.61(2)[w]	0.01	25,861.983(8)	-0.008	25,788.15(2)[b]	-0.02
21	25,957.81(7)[w b]	-0.03	25,876.59(2)[b]	-0.01	25,799.05(2)[b]	-0.02
22	25,976.74(6)[w b]	-0.03	25,891.86(3)[b]	-0.01	25,810.64(3)[b]	-0.02
23	25,996.40(4)[w]	0.01	25,907.83(2)	-0.01	25,822.94(2)	-0.01
24	26,016.69(5)[w b]	-0.03	25,924.51(3)	0.01	25,835.93(2)	-0.01
25	-		25,941.87(2)[w]	-0.01	25,849.64(3)[w b]	-0.01
26	-		25,960.01(3)[b]	0.01	25,864.12(2)[w]	0.01
27	-		25,980.1 (1)[w b]	-0.1	25,880.6(1)[w b]	0.1
28	-		25,997.81(8)[w b]	0.02	25,894.57(6)[w b]	0.01
29	-		26,018.03(5)[w b]	-0.01	25,911.16(2)[w]	0.01
30	-		26,038.94(6)[w b]	0.01	25,928.38(6)[w b]	0.01
31	-		-		25,946.27(6)[w b]	-0.03

[a] In units of cm^{-1}. The instrumental resolution was 0.018 cm^{-1}. The uncertainties in parentheses indicate 1σ standard deviations being combinations of the random (fitting) and systematic (calibration) errors. The estimated absolute calibration uncertainty was 0.004 cm^{-1}. The absolute accuracy of the line frequency measurements was estimated to be 0.01 – 0.04 cm^{-1} depending on the line intensity and blending.
[b] Lines marked with *b* and/or *w* are blended and/or weak.

Table 4
Extra-lines observed in the VIS-FT emission spectra.[a,b,c]

J''	$^{r}R_{11ee}$	o-c	$^{r}Q_{11ef}$	o-c	$^{q}Q_{11ef}$	o-c	$^{p}P_{11ee}$	o-c	$^{r}R_{12ee}$	o-c	$^{p}P_{12ee}$	o-c	$^{p}Q_{13ef}$	o-c
							$B^1\Sigma^+$ - $a'^3\Sigma^+$ (0, 10)							
11			20,750.12(3)[w,b]	0.01										
12			20,772.151(6)[b]	-0.004										
13														
14									20,838.84(1)	0.02	20,731.37(1)	0.01		
15									20,867.39(2)	-0.03				
16											20,772.12(1)[b]	-0.04		
17													20,814.35(2)[b]	0.02
18													20,840.078(6)	0.001
							$B^1\Sigma^+$ - $D^1\Delta$ (0, 1)							
27	21,080.21(2)	-0.02			20,976.877(7)[b]	0.005	20,877.15(1)[b]	0.01						
							$B^1\Sigma^+$ - $I^1\Sigma^-$(0, 2)							
35					21,150.10(2)[b]	-0.01								
							$B^1\Sigma^+$ - $a'^3\Sigma^+$ (1, 10)							
12			22,801.86(3)[w,b]	-0.03										
…														
14									22,866.50(6)[w,b]	0.02	22,760.432(4)[w,b]	-0.005		
							$C^1\Sigma^+$ - $a'^3\Sigma^+$ (0, 10)							
12			25,773.68(2)	-0.02										
…														
14											25,732.79(3)[w]	-0.01		
							$C^1\Sigma^+$ - $D^1\Delta$ (0, 1)							
27					25,976.25(7)[w,b]	-0.01								

[a] In units of cm^{-1}. The uncertainties in parentheses indicate 1σ standard deviations being combinations of the random (fitting) and systematic (calibration) errors.
[b] Lines marked with *b* and/or *w* are blended and/or weak.
[c] The branch-label subscripts *e* and *f* indicated the upper-/lower-state symmetry and superscripts *p*, *q* and *r* denote change in the total angular momentum excluding spin.

Table 5
Transition frequencies of the $^{12}C^{18}O$ $A^1\Pi$ – $X^1\Sigma^+(1, 0)$ absorption band obtained in the VUV-FT experiment.[a]

J"	R(J")	o-c	Q(J")	o-c	P(J")	o-c
0	66,205.13(1)	-0.02	-		-	
1	66,207.489(7)	-0.008	66,201.47(1)	-0.01	-	
2	66,209.185(7)	-0.009	66,200.164(7)	-0.009	66,194.15(1)	-0.02
3	66,210.227(7)	-0.008	66,198.20(1)	-0.01	66,189.180(7)[b]	-0.008
4	66,210.612(7)[b]	-0.008	66,195.577(7)	-0.009	66,183.553(7)	-0.009
5	66,210.344(7)	-0.007	66,192.303(7)	-0.008	66,177.273(7)	-0.008
6	66,209.42(1)[b]	-0.009	66,188.371(7)	-0.008	66,170.338(7)	-0.008
7	66,207.838(7)	-0.009	66,183.784(7)	-0.008	66,162.751(7)	-0.007
8	66,205.600(7)	-0.008	66,178.540(7)	-0.007	66,154.507(7)	-0.009
9	66,202.699(7)	-0.008	66,172.628(7)	-0.007	66,145.612(7)	-0.009
10	66,199.127(7)	-0.009	66,166.030(7)	-0.006	66,136.061(7)	-0.007
11	66,194.86(1)	-0.01	66,158.638(7)	-0.005	66,125.850(7)	-0.008
12	66,189.80(1)	-0.01	66,152.77(1)	-0.02	66,114.970(7)	-0.008
13	66,183.15(1)	-0.02	66,143.05(1)	-0.02	66,103.40(1)	-0.01
14	66,179.645(7)	-0.007	66,133.75(1)	-0.02	66,091.04(1)	-0.01
15	66,172.370(7)	-0.007	66,123.88(1)	-0.02	66,077.09(1)	-0.02
16	66,164.785(7)[b]	-0.006	66,113.33(1)	-0.02	66,066.290(7)	-0.007
17	66,156.62(1)	-0.02	66,101.90(1)	-0.03	66,051.725(7)	-0.007
18	66,147.83(1)	-0.01	66,091.405(7)	0.005	66,036.855(7)	-0.006
19	66,138.39(1)	-0.02	66,078.536(8)	-0.008	66,021.41(1)	-0.02
20	66,128.31(1)	-0.02	66,065.393(8)	-0.008	66,005.35(1)	-0.01
21	66,117.57(1)	-0.03	66,051.64(1)	-0.02	65,988.63(1)[w]	-0.02
22	66,106.19(1)	-0.02	66,037.26(1)	-0.03	65,971.29(1)[w]	-0.02
23	66,094.12(2)	-0.03	66,022.24(1)	-0.02	65,953.29(1)[w]	-0.03
24	-		66,006.55(2)	-0.01	65,934.66(1)[w]	-0.02
25	-		65,990.18(2)	-0.02	65,915.34(2)[w]	-0.03
26	-		65,973.12(4)	-0.01	-	

[a] In cm^{-1}. The instrumental resolution was 0.08 cm^{-1}. The uncertainties in parentheses indicate 1σ standard deviations being combinations of the random (fitting) and systematic (calibration) errors. The estimated absolute calibration uncertainty was 0.007 cm^{-1}. The absolute accuracy of the line frequency measurements was estimated to be 0.001–0.04 cm^{-1} depending on the line intensity and blending.
[b] Lines marked with *b* and/or *w* are blended and/or weak.

~ 115 nm. The transmitted signal is detected with the wavefront-division, VUV-FT spectrometer which is a permanent end station on the DESIRS beamline and has a maximum resolving power of 10^6. For studying shorter wavelengths, the windowed cell can be replaced with a windowless high-temperature cell limited to a maximum column density by the requirements of maintaining the beamline vacuum through differential pumping. The simple yet effective in-vacuum high-temperature absorption cell [55] consists of a 40 cm - long 7.5 × 4.5 mm rectangular-cross section tube wrapped with heating wire. This assembly is pressed within two semi-cylindrical shells to improve the uniformity of heating and the resulting rotational-excitation of CO gas measured in the cell is found to be well-described by a Boltzmann population at a single temperature. Multiple measurements were taken for each band with column density and temperature ranging between 2×10^{14} and 6×10^{16} cm^{-2}, and 300 or 900 K, respectively, in order to accurately measure lines of both low- and high-rotational excitation with moderate absorption depths. The recorded absorption bands are analysed line-by-line with a full accounting of their lineshapes, instrumental effects, and contaminating absorption by hot bands and other isotopologues.

An absolute frequency calibration is made uniformly to all measured spectra showing $B^1\Sigma^+ \longleftarrow X^1\Sigma^+$ and $C^1\Sigma^+ \longleftarrow X^1\Sigma^+$ by comparison with a highly-accurate absolute measurement of the Xe $5p^6$-$5p^5 8s^2[3/2]$ transition at 110 nm by Dreissen et al. [56]. This line appears in our spectra because of a Xe gas-filter chamber located upstream and used to remove higher-frequency harmonics generated by the beamline undulator. Only the ^{132}Xe isotope was studied by Dreissen et al. [56], but a previous measurement resolving the isotope splitting of nearby Xe lines [57] indicates the error introduced by using a pure ^{132}Xe standard to calibrate our natural-abundance experimental mixture is negligible. Comparison of our Xe-based frequency calibration with known overlapping lines of $^{12}C^{16}O$ B(0) ⟵ X(0) [58] shows agreement within 0.01 cm^{-1}. Our spectra showing $A^1\Pi(v = 1) \longleftarrow X^1\Sigma^+(v = 0)$ absorption were absolutely calibrated against contaminating $^{12}C^{16}O$ with reference to Niu et al. [40]. We estimate our absolute frequency calibration to be accurate to within 0.01 cm^{-1}.

Fig. 4 shows representative spectra recorded for each band and reveals uncomplicated $^1\Sigma^+$ – $^1\Sigma^+$ and $^1\Pi$ – $^1\Sigma^+$ rotational structure. Weak absorption due to $^{12}C^{16}O$ appears in several cases and was used to reinforce the frequency calibration of $^{12}C^{18}O$ bands. The transition frequencies of lines in the A(1) ⟵ X(0), B(0) ⟵ X(0), B(1) ⟵ X(0), and C(0) ⟵ X(0) bands are given in Tables 5, 6, 7, and 8, respectively. Strong extra lines attributable to a'(10) ⟵ X(0) appear in the spectrum of A(1) ⟵ X(0), as shown in Fig. 4 and their wavenumbers are gathered in Table 9. Apparent local perturbations of selected rotational transitions within the B(*v*) ⟵ X(0) and C(0) ⟵ X(0) bands have line shifts in the order of 0.02 to 0.1 cm^{-1} and are too small to stand out in Fig. 4. The 900 K spectra also exhibit hot bands due to B(1) ⟵ X(1), B(2) ⟵ X(1), and C(1) ⟵ X(1).

Results for the B(0) ⟵ X(0) band presented here are only marginally different to our previous analysis of this band in Trivikram et al. [22]. The updated frequency calibration described above lead to an increase of all frequencies by 0.01 cm^{-1}. Our analysis of the B ⟵ X and C ⟵ X absorption bands improves upon the similar experimental study of Lemaire et al. [32], also using the DESIRS beamline. This re-analysis was necessary in order that these bands are known with a precision matching our measured VIS-FT B → A and C → A line frequencies (having uncertainties down to 0.005 cm^{-1}) and sufficient to resolve the local line shifts due to energy level perturbations affecting B(*v*) and C(1) levels. In the new analysis, the statistical B ⟵ X and C ⟵ X line-frequency errors are approximately 0.002 cm^{-1}, whereas the random scattering of B(0), B(1), and C(0) energies in the previous work are

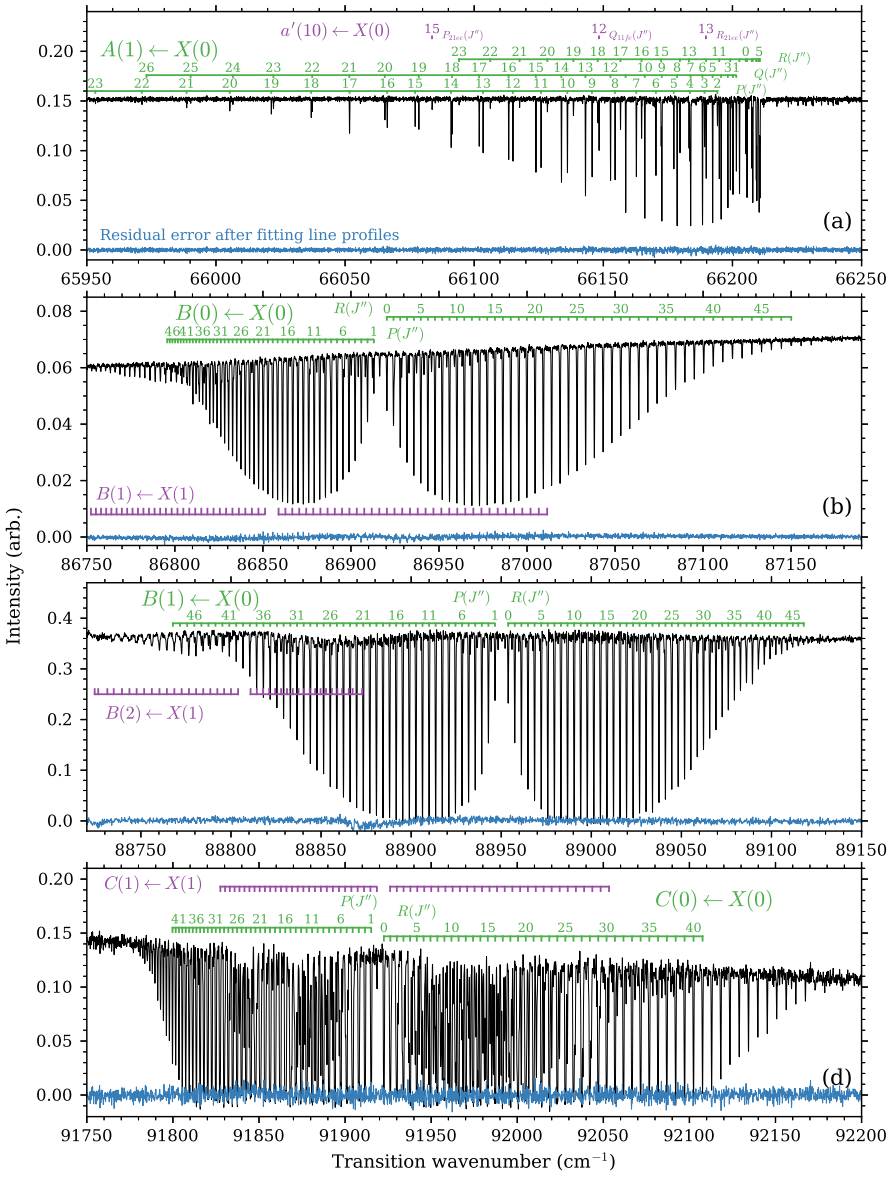

Fig. 4. High-resolution absorption spectra recorded with the VUV-FT experiment at SOLEIL. Spectrum (a), showing $^{12}C^{18}O$ $A^1\Pi \longleftarrow X^1\Sigma^+(1, 0)$, was recorded at room temperature and includes extra lines due the interaction between A(1) and a'(10). Spectra (b), (c), and (d), presenting the $B^1\Sigma^+ \longleftarrow X^1\Sigma^+(0, 0)$, $B^1\Sigma^+ \longleftarrow X^1\Sigma^+(1, 0)$, and $C^1\Sigma^+ \longleftarrow X^1\Sigma^+(0, 0)$ bands, are recorded at 900 K and include measurable absorption from X(1). Weak unassigned lines are due to contamination by $^{12}C^{16}O$.

approximately 0.01, 0.01, 0.005 cm^{-1}, respectively, The improvement was achieved using new absorption spectra recorded at an improved signal-to-noise ratio and by simultaneously fitting B(0), B(1), and C(0) level energies to spectra recorded at a range of temperatures and pressures. Fitting upper-level energies directly, and adopting fixed reference ground-state energy levels [59], also permitted the correlated fitting of *P*- and *R*-branch lines with common upper levels as well as the corresponding absorption to X(1) hot bands. Higher-*J* rotational levels than previously analysed are present in the new high-temperature absorption spectra. We also find overall energy shifts for the B(0), B(1), and C(0) vibrational levels relative to Lemaire et al. [32], of -0.05, -0.05, and 0.025 cm^{-1}, respectively, based on an absolute frequency calibration using the Xe reference data described above and benefiting from the simultaneous self-consistent fitting of overlapping spectra covering all bands. Small irregularities in the level energy progressions of $^{12}C^{18}O$ $B^1\Sigma^+(v = 0, 1)$ and $C^1\Sigma^+(v = 0)$ levels are indicated in Fig. 5. Here, term values are computed from the observed levels and plotted after subtraction of their general rotational dependence as modelled by a polynomial in terms of $J(J+1)^n$.

3. Deperturbation analysis

The $A^1\Pi$ electronic state of carbon monoxide is extensively perturbed in all isotopologues as a result of interactions with several electronic states: homogeneous spin-orbit interactions with the $a'^3\Sigma^+$, $e^3\Sigma^-$, $d^3\Delta$ triplet states, and heterogeneous ***L*-**uncoupling rotation-electronic interactions with the $I^1\Sigma^-$ and $D^1\Delta$ singlet states [39,60–62].

We assembled a preliminary model of these interactions in $^{12}C^{18}O$ that approximately reproduces the measured emission and absorption ro-vibronic transitions of $A^1\Pi(v = 1)$ and the extra forbidden lines attributed to levels perturbing A(1) and thereby attaining some transition strength. Values of the necessary molecular

Table 6
Transition frequencies of the $^{12}C^{18}O$ $B^1\Sigma^+$ – $X^1\Sigma^+(0, 0)$ absorption band obtained in the VUV-FT experiment.[a]

J''	R(J'')	o-c	P(J'')	o-c
0	86,920.41(1)	0.02	-	
1	86,924.17(1)	0.02	86,913.03(1)	0.01
2	86,927.97(1)	0.02	86,909.42(1)	0.02
3	86,931.83(1)	0.02	86,905.86(1)	0.02
4	86,935.74(1)	0.02	86,902.34(1)	0.02
5	86,939.69(1)	0.02	86,898.88(1)	0.02
6	86,943.69(1)	0.02	86,895.46(1)	0.02
7	86,947.74(1)	0.02	86,892.10(1)	0.02
8	86,951.83(1)	0.03	86,888.78(1)	0.02
9	86,955.98(1)	0.03	86,885.51(1)	0.02
10	86,960.16(1)	0.03	86,882.30(1)	0.03
11	86,964.39(1)	0.02	86,879.13(1)	0.03
12	86,968.68(1)	0.02	86,876.01(1)	0.02
13	86,973.02(1)	0.02	86,872.93(1)	0.02
14	86,977.39(1)	0.02	86,869.92(1)	0.02
15	86,981.81(1)	0.02	86,866.96(1)	0.02
16	86,986.27(1)	0.02	86,864.03(1)	0.02
17	86,990.78(1)	0.03	86,861.16(1)	0.02
18	86,995.33(1)	0.02	86,858.34(1)	0.02
19	86,999.92(1)	0.02	86,855.57(1)	0.03
20	87,004.56(1)	0.02	86,852.84(1)	0.02
21	87,009.25(1)	0.02	86,850.17(1)	0.02
22	87,013.98(1)	0.02	86,847.54(1)	0.02
23	87,018.75(1)	0.02	86,844.96(1)	0.02
24	87,023.55(1)	0.01	86,842.44(1)	0.02
25	87,028.40(1)	0.01	86,839.96(1)	0.02
26	87,033.29(1)	0.01	86,837.53(1)	0.01
27	87,038.23(1)	0.01	86,835.14(1)	0.01
28	87,043.21(1)	0.01	86,832.81(1)	0.01
29	87,048.21(1)	0.01	86,830.52(1)	0.01
30	87,053.26(1)	0.01	86,828.29(1)	0.01
31	87,058.35(1)	0.01	86,826.09(1)	0.01
32	87,063.47(1)	0.01	86,823.95(1)	0.01
33	87,068.61(1)	0.01	86,821.84(1)	0.01
34	87,073.84(1)	-0.01	86,819.79(1)[b]	0.01
35	87,079.07(1)	0.01	86,817.76(1)	0.01
36	87,084.35(1)	0.01	86,815.82(1)	-0.01
37	87,089.64(1)	-0.01	86,813.90(1)[b]	0.01
38	87,094.98(1)	-0.01	86,812.04(1)	0.01
39	87,100.35(1)	0.00	86,810.20(1)[b]	-0.01
40	87,105.75(1)	0.00	86,808.42(1)	-0.01
41	87,111.20(1)	0.00	86,806.68(1)[b]	0.00
42	87,116.66(1)	0.00	86,804.98(1)	0.00
43	87,122.15(1)	0.00	86,803.33(1)[w]	0.00
44	87,127.68(1)	0.00	86,801.72(1)[w]	0.00
45	87,133.22(1)	0.00	86,800.14(1)[w]	0.00
46	87,138.81(1)	0.00	86,798.61(1)[w]	0.00
47	87,144.40(1)[w]	0.00	86,797.11(1)[w b]	0.00
48	87,150.03(1)[w]	0.00	86,795.67(1)[w b]	0.00

[a] In cm^{-1}. The instrumental resolution was 0.15 cm^{-1}. The uncertainties in parentheses indicate 1σ standard deviations being combinations of the random (fitting) and systematic (calibration) errors. The estimated absolute calibration uncertainty was 0.01 cm^{-1}. The absolute accuracy of the line frequency measurements was estimated to be 0.003–0.008 cm^{-1} depending on the line intensity and blending.
[b] Lines marked with *b* and/or *w* are blended and/or weak.

Table 7
Transition frequencies of the $^{12}C^{18}O$ $B^1\Sigma^+$ – $X^1\Sigma^+(1, 0)$ absorption band obtained in the VUV-FT experiment.[a]

J''	R(J'')	o-c	P(J'')	o-c
0	88,953.86(1)	-0.01	-	
1	88,957.52(1)	0.01	88,946.54(1)	0.00
2	88,961.18(1)	0.01	88,942.87(1)	-0.01
3	88,964.84(1)	0.01	88,939.21(1)	0.01
4	88,968.50(1)	0.01	88,935.55(1)	0.01
5	88,972.18(1)	0.01	88,931.89(1)	0.01
6	88,975.84(1)	0.01	88,928.23(1)	0.01
7	88,979.49(1)	0.01	88,924.58(1)	0.01
8	88,983.15(1)	0.02	88,920.93(1)	0.01
9	88,986.81(1)	0.01	88,917.27(1)	0.01
10	88,990.46(1)	0.02	88,913.61(1)	0.02
11	88,994.11(1)	0.01	88,909.96(1)	0.01
12	88,997.76(1)	0.02	88,906.30(1)	0.02
13	89,001.40(1)	0.01	88,902.65(1)	0.01
14	89,005.05(1)	0.01	88,899.00(1)	0.02
15	89,008.68(1)	0.01	88,895.34(1)	0.01
16	89,012.31(1)	0.01	88,891.69(1)	0.01
17	89,015.94(1)	0.02	88,888.04(1)	0.01
18	89,019.56(1)	0.01	88,884.38(1)	0.01
19	89,023.18(1)	0.00	88,880.73(1)	0.02
20	89,026.78(1)	0.01	88,877.07(1)	0.01
21	89,030.38(1)	0.00	88,873.42(1)	0.00
22	89,033.97(1)	0.00	88,869.76(1)	0.01
23	89,037.55(1)	0.00	88,866.10(1)	0.00
24	89,041.11(1)	0.00	88,862.43(1)	0.00
25	89,044.67(1)	0.00	88,858.76(1)	0.00
26	89,048.22(1)	0.00	88,855.09(1)	0.00
27	89,051.74(1)	0.00	88,851.41(1)	0.00
28	89,055.26(1)	0.00	88,847.73(1)	0.00
29	89,058.77(1)	0.00	88,844.04(1)	0.00
30	89,062.26(1)	0.00	88,840.35(1)	0.00
31	89,065.73(1)	0.00	88,836.65(1)	0.00
32	89,069.18(1)	0.00	88,832.95(1)	0.00
33	89,072.62(1)	0.00	88,829.22(1)	0.00
34	89,076.02(1)	0.00	88,825.50(1)	0.00
35	89,079.42(1)	0.00	88,821.76(1)	0.00
36	89,082.77(1)	0.00	88,818.01(1)	0.00
37	89,086.13(1)	0.00	88,814.25(1)	0.00
38	89,089.45(1)	0.00	88,810.46(1)	0.00
39	89,092.73(1)	0.00	88,806.69(1)	0.00
40	89,096.00(1)	0.00	88,802.89(1)	0.00
41	89,099.26(1)	0.00	88,799.06(1)	0.00
42	89,102.42(2)	0.00	88,795.23(1)	0.00
43	89,105.60(2)	0.00	88,791.40(1)[w]	0.00
44	89,108.71(2)[w]	0.00	88,787.48(2)[w]	0.00
45	89,111.81(3)[w b]	0.00	88,783.59(2)[w]	0.00
46	89,114.85(3)[w b]	0.00	88,779.65(2)[w b]	0.00
47	89,117.91(4)[w b]	0.00	88,775.70(3)[w b]	0.00
48	-		88,771.71(3)[w b]	0.00
49	-		88,767.76(4)[w b]	0.00

[a] In cm^{-1}. The instrumental resolution was 0.15 cm^{-1}. The uncertainties in parentheses indicate 1σ standard deviations being combinations of the random (fitting) and systematic (calibration) errors. The estimated absolute calibration uncertainty was 0.01 cm^{-1}. The absolute accuracy of the line frequency measurements was estimated to be 0.003–0.04 cm^{-1} depending on the line intensity and blending.
[b] Lines marked with *b* and/or *w* are blended and/or weak.

parameters are based on literature data for $^{12}C^{18}O$ [21,30,34,38,59,61,63–69] or isotopically scaled from other isotopologues and result in the level diagram shown in Fig. 6. This figure clearly identifies which level-crossings and nearby states are likely to perturb $A^1\Pi(v = 1)$. The potentially-perturbing vibrational levels are $e^3\Sigma^-(v = 0 - 4)$, $d^3\Delta(v = 3 - 7)$, $a'^3\Sigma^+(v = 8 - 12)$, $D^1\Delta(v = 0 - 2)$, $I^1\Sigma^-(v = 0 - 4)$, and $a^3\Pi(v = 11 - 12)$. Matrix elements for all possible spin-orbit and rotational interactions between these levels and A(1) were introduced into a comprehensive model and an evaluation made of their direct and indirect influence on the measured line frequencies. A summary discussion for all 47 interactions considered appears in Table 10 and only those having a meaningful influence are subsequently taken into account.

A final deperturbation analysis of $^{12}C^{18}O$ A(1) was conducted using a development version of the PGOPHER software [50,51]. The constraining experimental data consists of 626 transitions from the $B^1\Sigma^+ - A^1\Pi(0, 1)$, (1, 1) and $C^1\Sigma^+ - A^1\Pi(0, 1)$ bands obtained by VIS-FT emission spectroscopy and the $A^1\Pi - X^1\Sigma^+(1, 0)$, $B^1\Sigma^+ - X^1\Sigma^+(0, 0)$, $B^1\Sigma^+ - X^1\Sigma^+(1, 0)$, and $C^1\Sigma^+ - X^1\Sigma^+(0, 0)$ bands recorded by VUV-FT absorption. The A(1) state and its perturbers were modelled with an effective Hamiltonian [50,51], while the $B^1\Sigma^+$ and $C^1\Sigma^+$ upper states are retained as lists of term values because of the unidentified perturbations responsible for their

Table 8
Transition frequencies of the $^{12}C^{18}O$ $C^1\Sigma^+$ – $X^1\Sigma^+(0, 0)$ absorption band obtained in the VUV-FT experiment.[a]

J"	R(J")	o-c	P(J")	o-c
0	91,922.54(1)	0.01	-	
1	91,926.28(1)	0.01	91,915.17(1)	0.01
2	91,930.06(1)	0.01	91,911.55(1)	0.01
3	91,933.89(1)	0.02	91,907.97(1)	0.01
4	91,937.75(1)	0.01	91,904.43(1)	0.01
5	91,941.66(1)	0.01	91,900.93(1)	0.02
6	91,945.60(1)	0.02	91,897.48(1)	0.01
7	91,949.59(1)	0.02	91,894.06(1)	0.01
8	91,953.61(1)	0.01	91,890.69(1)	0.02
9	91,957.68(1)	0.02	91,887.36(1)	0.02
10	91,961.78(1)	0.02	91,884.07(1)	0.01
11	91,965.92(1)	0.01	91,880.83(1)	0.02
12	91,970.11(1)	0.01	91,877.62(1)	0.02
13	91,974.33(1)	0.02	91,874.46(1)	0.01
14	91,978.59(1)	0.01	91,871.34(1)	0.01
15	91,982.89(1)	0.01	91,868.27(1)	0.02
16	91,987.22(1)	0.01	91,865.23(1)	0.01
17	91,991.59(1)	0.01	91,862.24(1)	0.01
18	91,996.01(1)	0.02	91,859.29(1)	0.01
19	92,000.46(1)	0.02	91,856.38(1)	0.01
20	92,004.95(1)	0.01	91,853.52(1)	0.02
21	92,009.47(1)	0.01	91,850.71(1)	0.02
22	92,014.04(1)	0.01	91,847.93(1)	0.01
23	92,018.64(1)	-0.01	91,845.19(1)	0.01
24	92,023.28(1)	0.01	91,842.50(1)	0.01
25	92,027.95(1)	-0.01	91,839.85(1)	-0.01
26	92,032.67(1)	0.01	91,837.26(1)	0.01
27	92,037.41(1)	-0.01	91,834.69(1)	-0.01
28	92,042.20(1)	0.01	91,832.18(1)	0.01
29	92,047.02(1)	0.01	91,829.71(1)	-0.01
30	92,051.88(1)	0.00	91,827.28(1)	0.01
31	92,056.77(1)	0.00	91,824.90(1)	0.01
32	92,061.70(1)	0.00	91,822.57(1)	0.00
33	92,066.67(1)	0.00	91,820.26(1)	0.00
34	92,071.67(1)	0.00	91,818.02(1)	0.00
35	92,076.70(1)	0.00	91,815.82(1)[w]	0.00
36	92,081.78(1)	0.00	91,813.65(1)[w]	0.00
37	92,086.88(1)	0.00	91,811.54(1)[w]	0.00
38	92,092.02(1)[w]	0.00	91,809.47(1)[w]	0.00
39	92,097.19(1)[w]	0.00	91,807.44(1)[w]	0.00
40	92,102.39(1)[w]	0.00	91,805.46(1)[w]	0.00
41	92,107.63(1)[w]	0.00	91,803.52(1)[w]	0.00
42	-		91,801.62(1)[w]	0.00
43	-		91,799.77(1)[w]	0.00

[a] In cm^{-1}. The instrumental resolution was 0.15 cm^{-1}. The uncertainties in parentheses indicate 1σ standard deviations being combinations of the random (fitting) and systematic (calibration) errors. The estimated absolute calibration uncertainty was 0.01 cm^{-1}. The absolute accuracy of the line frequency measurements was estimated to be 0.001–0.006 cm^{-1} depending on the line intensity and blending.[b]Lines marked with *b* and/or *w* are blended and/or weak.

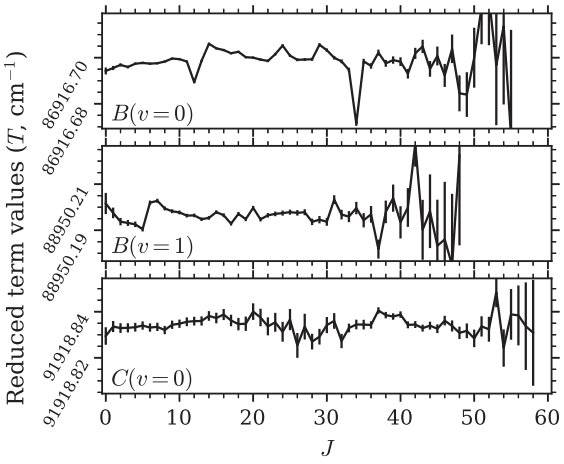

Fig. 5. Reduced term values of the B(v) and C(v = 0) levels computed from their measured line frequencies and the ground state energy levels of [59], and after subtraction of their $J(J+1)^n$ dependence for n = 1, 2, and 3. Error bars indicate the estimated random standard error due to line fitting.

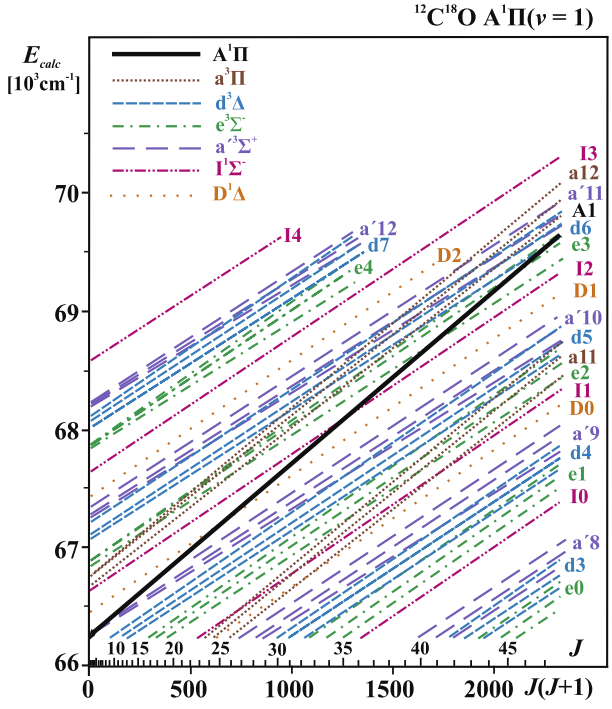

Fig. 6. Diagram of the ro-vibronic terms in the surrounding (66,000 – 70,000 cm^{-1}) region of $A^1\Pi(v = 1)$. Labels indicate the electronic states and to their right - vibrational quantum numbers.

Table 9
Extra-lines observed in the VUV-FT absorption spectra.[a,b,c]

J"	$^pQ_{11fe}$	o-c	$^rR_{21ee}$	o-c	$^pP_{21ee}$	o-c
			$a'^3\Sigma^+$ – $X^1\ \Sigma^+$ (10, 0)			
12	66,148.318(7)	0.001				
13			66,189.729(8)[b]	-0.03		
...						
15					66,083.668(8)	-0.03

[a] In units of cm^{-1}. The uncertainties in parentheses indicate 1σ standard deviations being combinations of the random (fitting) and systematic (calibration) errors.
[b] Lines marked with *b* are blended.
[c] The branch-label subscripts *e* and *f* indicated the upper-/lower-state symmetry and superscripts *p* and *r* denote change in the total angular momentum excluding spin.

Table 10
Interactions verified during the $^{12}C^{18}O$ $A^1\Pi(v=1)$ deperturbation analysis.

Nº	Tested interactions		Nature of the perturbation	Included in the fit	Status[a]	Characteristics of the interaction
1	$A^1\Pi(v=1)$	~$a'^3\Sigma^+(v=8)$	Spin-orbit	No	-	Negligible.
2		~$a'^3\Sigma^+(v=9)$	"	No	-	Negligible.
3		~$a'^3\Sigma^+(v=10)$	"	Yes	Floated	-
4		~$a'^3\Sigma^+(v=11)$	"	Yes	Fixed	Significant, nevertheless statistically unjustified (without meaningful correlations).
5		~$a'^3\Sigma^+(v=12)$	"	No	-	Negligible.
6		~$e^3\Sigma^-(v=0)$	"	No	-	Negligible.
7		~$e^3\Sigma^-(v=1)$	"	Yes	Fixed	Noticeable but very small influence. Statistically unjustified. If floated, it correlates with D of A(1) and <A(1)|**LS**|e(3)> and <A(1)|**LS**|d(5)> as well as causes correlations between <A(1)|**LS**|d(6)> and <A(1)|**LS**|e(1)>.
8		~$e^3\Sigma^-(v=2)$	"	Yes	Fixed	Significant. It causes divergence of the fit If floated.
9		~$e^3\Sigma^-(v=3)$	"	Yes	Floated	-
10		~$e^3\Sigma^-(v=4)$	"	No	-	Negligible.
11		~$d^3\Delta(v=3)$	"	No	-	Negligible.
12		~$d^3\Delta(v=4)$	"	Yes	Fixed	Noticeable, but very small influence. Statistically unjustified. If floated, it correlates with D constant of A(1), <A(1)|**LS**|d(4)>, <A(1)|**LS**|d(5)>, and <A(1)|**LS**|d(6)>.
13		~$d^3\Delta(v=5)$	"	Yes	Floated	-
14		~$d^3\Delta(v=6)$	"	Yes	Fixed	Significant. If floated, the fitted value deviates significantly from the calculated one (anti-crossing appears too far from the experimental levels).
15		~$d^3\Delta(v=7)$	"	No	-	Statistically unjustified.
16		~$D^1\Delta(v=0)$	Rotation-electronic (L-uncoupling)	No	-	Negligible.
17		~$D^1\Delta(v=1)$	"	Yes	Floated	-
18		~$D^1\Delta(v=2)$	"	No	-	Negligible.
19		~$I^1\Sigma^-(v=0)$	"	Yes	Fixed	Significant, nevertheless statistically unjustified (without meaningful correlations).
20		~$I^1\Sigma^-(v=1)$	"	Yes	Floated	-
21		~$I^1\Sigma^-(v=2)$	"	Yes	Floated	-
22		~$I^1\Sigma^-(v=3)$	"	Yes	Fixed	Small influence. If floated, it correlates with <A(1)|$\mathbf{J}_+\mathbf{L}_-$|I(1)>.
23		~$I^1\Sigma^-(v=4)$	"	No	-	Negligible.
24	$d^3\Delta(v=5)$	~$a'^3\Sigma^+(v=10)$	Spin-spin	No	-	Noticeable but very small indirect influence on A(1). If floated, it correlates with <A(1)|**LS**|a$\acute{}$(10)>.
25		~$e^3\Sigma^-(v=2)$	"	No	-	Statistically unjustified (without meaningful correlations).
26	$d^3\Delta(v=6)$	~$a'^3\Sigma^+(v=11)$	"	No	-	Statistically unjustified (without meaningful correlations).
27		~$e^3\Sigma^-(v=3)$	"	No	-	Statistically unjustified. If floated, it correlates with B and D constants of A(1) and <A(1)|**LS**|e(3)>and <A(1)|**LS**|d(5)>.
28	$a'^3\Sigma^+(v=10)$	~$e^3\Sigma^-(v=2)$	Spin-orbit	No	-	Statistically unjustified. If floated, it correlates with B and γ constants of a$\acute{}$(10) and <A(1)|**LS**|a$\acute{}$(10)>.
29	$a'^3\Sigma^+(v=11)$	~$e^3\Sigma^-(v=3)$	"	No	-	Statistically unjustified (without meaningful correlations).
30	$a^3\Pi(v=11)$	~$d^3\Delta(v=5)$	Spin-orbit/spin-electronic/L-uncoupling	No	-	Negligible indirect influence on A(1).
31		~$d^3\Delta(v=6)$	"	No	-	Negligible indirect influence on A(1).
32		~$e^3\Sigma^-(v=2)$	"	No	-	Negligible indirect influence on A(1).
33		~$e^3\Sigma^-(v=3)$	"	No	-	Negligible indirect influence on A(1).
34		~$a'^3\Sigma^+(v=10)$	"	No	-	Negligible indirect influence on A(1).
35		~$a'^3\Sigma^+(v=11)$	"	No	-	Negligible indirect influence on A(1).
36		~$I^1\Sigma^-(v=1)$	Spin-orbit	No	-	Negligible indirect influence on A(1).
37		~$I^1\Sigma^-(v=2)$	"	No	-	Negligible indirect influence on A(1).
38		~$D^1\Delta(v=1)$	"	No	-	Negligible indirect influence on A(1).
39	$a^3\Pi(v=12)$	~$d^3\Delta(v=5)$	Spin-orbit /spin-electronic/L-uncoupling	No	-	Negligible indirect influence on A(1).
40		~$d^3\Delta(v=6)$	"	No	-	Negligible indirect influence on A(1).
41		~$e^3\Sigma^-(v=2)$	"	No	-	Negligible indirect influence on A(1).
42		~$e^3\Sigma^-(v=3)$	"	No	-	Negligible indirect influence on A(1).
43		~$a'^3\Sigma^+(v=10)$	"	No	-	Negligible indirect influence on A(1).
44		~$a'^3\Sigma^+(v=11)$	"	No	-	Negligible indirect influence on A(1).
45		~$I^1\Sigma^-(v=1)$	Spin-orbit	No	-	Negligible indirect influence on A(1).
46		~$I^1\Sigma^-(v=2)$	"	No	-	Negligible indirect influence on A(1).
47		~$D^1\Delta(v=1)$	"	No	-	Negligible indirect influence on A(1).

[a] "Fixed" means, that the parameter is constrained to the theoretical value during the final fit.

Table 11
Deperturbed molecular parameters of the $^{12}C^{18}O$ $A^1\Pi(v = 1)$ level and its perturbers.[a,b]

Constant	$A^1\Pi(v = 1)$	$A^1\Pi(v = 1)$ Ref. [28]	$A^1\Pi(v = 1)$ Ref. [26]	$a'^3\Sigma^+(v = 10)$	$a'^3\Sigma^+(v = 10)$ Ref. [28]	$a'^3\Sigma^+(v = 10)$ Ref. [26]	$a'^3\Sigma^+(v = 11)$
T_v	66,201.23405(387)	66,202.8438(72)	66,202.946(6)	66,288.54800(454)	66,288.138(36)	66,288.2(1)	67,277.64[h]
B	1.50674738(848)	1.506559(33)	1.50658(3)	1.1121020(283)	1.11359	1.1140(7)	1.10[i]
$D \times 10^6$	6.78284(597)	6.65	6.8	5.68[i]	5.81	5.7	5.67[i]
$H \times 10^{12}$				-0.35[f]			-0.35[f]
λ				-1.1645(63)	-1.15	-1.1	-1.11[i]
$\gamma \times 10^2$				-1.782(40)		-0.72	-0.61[j]
η				-5.02609(417)	-5.014(28)[g]	-5.04(2)[g]	
$\eta_{theoret}$[c]				-5.03			3.78
$\delta\eta$[d]				0.03			
Constant	$D^1\Delta(v = 1)$	$D^1\Delta(v = 1)$ Ref. [28]	$D^1\Delta(v = 1)$ Ref. [26]	$I^1\Sigma^-(v = 0)$	$I^1\Sigma^-(v = 1)$	$I^1\Sigma^-(v = 2)$	$I^1\Sigma^-(v = 2)$ Ref. [28]
T_v	66,454.7292(77)	66,453.21	66,461.2(9)	64,558.8768[h]	65,604.21[h]	66,630.075(24)	66,630.36
B	1.17[k]	1.17241	1.17241	1.200838[i]	1.18[i]	1.168014[i]	1.16801
$D \times 10^6$	6.37[k]	6.39	6.3	6.21[l]	6.23[l]	6.25[l]	6.24
$H \times 10^{12}$	-0.26[i]			2.59[f]	2.59[f]	2.59[f]	
$\xi \times 10^2$	-7.023(16)	5.9[g]	-8.5(9)[g]		10.88(39)	-8.054(21)	5.3[g]
$\xi_{theoret} \times 10^2$ [c]	-6.29			-7.99	9.41	-7.36	
$\delta\xi$ [d]	11.6				15.6	9.4	
Constant	$I^1\Sigma^-(v = 3)$	$e^3\Sigma^-(v = 1)$	$e^3\Sigma^-(v = 2)$	$e^3\Sigma^-(v = 3)$	$d^3\Delta(v = 4)$	$d^3\Delta(v = 5)$	$d^3\Delta(v = 6)$
T_v	67,635.54[h]	64,787.67[h]	65,838.83[h]	66,870.98[h]	65,014.2[h]	66,061.47[h]	67,090.34[h]
B	1.15[i]	1.20[i]	1.18[i]	1.16[i]	1.18[i]	1.16[i]	1.14[i]
$D \times 10^6$	6.26[l]	6.18[i]	6.14[i]	6.10[i]	5.98[i]	5.86[i]	5.84[i]
$H \times 10^{12}$	2.59[f]	-1.73[f]	-1.73[f]	-1.73[f]	-0.69[f]	-0.69[f]	-0.69[f]
A					-16.54[i]	-16.32[i]	-16.47[i]
$A_D \times 10^5$					-0.1[j]	-4.83[j]	-4.83[j]
λ		0.53[m]	0.52[m]	0.53[m]	1.25[n]	0.88[n]	0.98[n]
$\gamma \times 10^2$		-0.21[e]			-0.85[j]	-0.79[j]	-0.08[j]
η				-4.686(287)		16.3582(414)	
$\eta_{theoret}$[c]		18.97	12.75	-4.41	11.03	16.48	18.17
$\delta\eta$[d]				6.2		0.7	
$\xi_{theoret} \times 10^2$ [c]	3.66						

[a] All values are in cm^{-1}, except for relative errors which are given in percentages.
[b] Floated parameters during the model optimisation are given with uncertainties in parentheses (1σ, in units of the last significant digit). All other parameters were fixed during the fitting procedure. All perturbation parameters refer to interactions with the A(1) level. Molecular constants of the $^{12}C^{18}O$ $X(v = 0)$ ground state were fixed to the values determined by Coxon and Hajigeorgiou [59].
[c] Theoretical spin-orbit and rotation-electronic interaction parameters calculated on the basis of isotopologue-independent perturbation parameters ***a*** and ***b*** (given by Hakalla et al. [43] for A~á and A~D interactions as well obtained using data from Ref. [61] for A~e, A~d and A~I perturbations) based on the Eqs.(1)-(5) from Ref. [49] and Eqs.(1)-(3) from this work. Calculations of the vibrational overlap integrals $\langle v_A | v_{e,d,a'} \rangle$ and rotational operator integrals $\langle v_A | \boldsymbol{B}(\boldsymbol{R}) | v_{I,D} \rangle$ were calculated in this work based on Ref. [43].
[d] Relative error: difference between theoretical and experimentally determined values in terms of a percentage: $\delta\eta = \frac{(\eta_{theoret} - \eta)}{\eta_{theoret}} \times 100\%$; $\delta\xi = \frac{(\xi_{theoret} - \xi)}{\xi_{theoret}} \times 100\%$
[e] Taken from Ref. [22].
[f] Obtained by isotopic scaling of the values taken from Ref. [61].
[g] The η and ξ parameters have been calculated on the basis of the α and β given in Ref. [26] or [28] using Eqs. (1) - (3).
[h] Obtained by isotopic scaling of the values taken from Refs. [38,59,63].
[i] Obtained by isotopic scaling of the values taken from Ref. [38].
[j] Taken from Ref. [38] (in MHz), converted into cm^{-1} and isotopically scaled.
[k] Obtained by isotopic scaling of the values taken from Ref. [64].
[l] Calculated in this work based on Ref. [61] and isotopic scaling procedure.
[m] The isotopically scaled, diagonal spin-spin constant $\lambda = -1.5 \times C$, where C was taken from Refs. [38,39].
[n] Calculated in this work on the basis of Ref. [38] and isotopic scaling procedure.

weak energy level irregularities [19,22,32,45,49,70] (see also Fig. 5). More details of the procedure used for least-squares fitting line frequencies to simultaneous determination of the molecular constants and term values are described in Refs. [71–74]. This procedure means that the unmodelled perturbations affecting the B and C levels have no influence on the deperturbed molecular constants of the A, a; e, d, D, or I levels during the fits. Following this analysis, the $A^1\Pi(v = 1)$ level and its perturbers as well as the $B^1\Sigma^+(v = 0, 1)$ and $C^1\Sigma^+(v = 0)$ levels are described by a fitted set of 157 independent parameters including: deperturbed molecular constants for $A^1\Pi(v = 1)$, $a'^3\Sigma^+(v = 10)$, $D^1\Delta$ $(v = 1)$, and $I^1\Sigma^-(v = 2)$ levels; the $A^1\Pi$ ~ ($a'^3\Sigma^+$, $e^3\Sigma^-$, $d^3\Delta$) spin-orbit interactions and the $A^1\Pi$ ~ ($D^1\Delta$, $I^1\Sigma^-$) ***L***-uncoupling interactions, parametrised by the η and ξ symbols, respectively, as well as term energies for the $B^1\Sigma^+(v = 0, 1)$ and $C^1\Sigma^+(v = 0)$ levels. The fitted molecular parameters are presented in Tables 11 and 12. The rotational operator in the PGOPHER Hamiltonian was taken as a power series expansion in the angular momentum operator excluding spin ($\hat{N}$). Definitions of the interaction parameters η and ξ are discussed in [43,45,49] and their relations to α and β perturbation parameters used in Refs. [26,28] are as follows:

$$\eta_i = -\alpha_i\sqrt{3}, \quad (1)$$

$$\xi_{A\sim I} = -\beta_{A\sim I}\sqrt{2}, \quad (2)$$

$$\xi_{A\sim D} = \beta_{A\sim D}, \quad (3)$$

where the subscript i indicates A ~ d, A ~ e or A ~ áinteractions.

Table 12
Term values of the $B^1\Sigma^+(v = 0, 1)$ and $C^1\Sigma^+(v = 0)$ levels in $^{12}C^{18}O$.[a,b]

J	$B^1\Sigma^+$ $(v = 0)$	$B^1\Sigma^+$ $(v = 1)$	$C^1\Sigma^+$ $(v = 0)$
0	86,916.687(8)	88,950.20(2)	91,918.83(2)
1	86,920.394(5)	88,953.860(8)	91,922.531(7)
2	86,927.815(4)	88,961.177(7)	91,929.940(8)
3	86,938.945(4)	88,972.163(8)	91,941.045(8)
4	86,953.785(3)	88,986.813(7)	91,955.848(6)
5	86,972.336(3)	89,005.118(7)	91,974.362(6)
6	86,994.595(3)	89,027.095(6)	91,996.574(6)
7	87,020.563(3)	89,052.721(6)	92,022.482(5)
8	87,050.236(3)	89,082.002(6)	92,052.093(6)
9	87,083.616(3)	89,114.942(5)	92,085.406(6)
10	87,120.699(3)	89,151.542(5)	92,122.409(6)
11	87,161.485(3)	89,191.790(6)	92,163.111(5)
12	87,205.969(3)	89,235.700(6)	92,207.509(5)
13	87,254.167(3)	89,283.246(4)	92,255.600(6)
14	87,306.053(3)	89,334.451(5)	92,307.371(5)
15	87,361.631(3)	89,389.302(6)	92,362.839(5)
16	87,420.904(3)	89,447.792(6)	92,421.995(6)
17	87,483.872(3)	89,509.922(6)	92,484.833(5)
18	87,550.516(3)	89,575.689(5)	92,551.347(6)
19	87,620.857(3)	89,645.097(6)	92,621.544(6)
20	87,694.881(3)	89,718.149(8)	92,695.425(6)
21	87,772.584(3)	89,794.808(8)	92,772.983(7)
22	87,853.963(3)	89,875.106(8)	92,854.201(7)
23	87,939.020(3)	89,959.022(8)	92,939.092(7)
24	88,027.748(3)	90,046.556(9)	93,027.650(8)
25	88,120.137(3)	90,137.706(9)	93,119.871(7)
26	88,216.191(4)	90,232.465(9)	93,215.741(9)
27	88,315.905(4)	90,330.832(9)	93,315.282(9)
28	88,419.270(4)	90,432.796(9)	93,418.462(8)
29	88,526.296(4)	90,538.363(9)	93,525.296(9)
30	88,636.968(4)	90,647.522(9)	93,635.779(9)
31	88,751.273(4)	90,760.279(9)	93,749.899(9)
32	88,869.224(5)	90,876.603(9)	93,867.644(9)
33	88,990.802(4)	90,996.511(9)	93,989.035(9)
34	89,115.990(6)	91,119.995(9)	94,114.049(9)
35	89,244.852(6)	91,247.038(9)	94,242.684(9)
36	89,377.302(6)	91,377.650(9)	94,374.937(9)
37	89,513.374(6)	91,511.799(9)	94,510.810(9)
38	89,653.046(6)	91,649.528(9)	94,650.282(9)
39	89,796.327(7)	91,790.79(1)	94,793.358(9)
40	89,943.195(9)	91,935.57(1)	94,940.033(9)
41	90,093.653(9)	92,083.90(1)	95,090.295(9)
42	90,247.710(9)	92,235.78(2)	95,244.148(9)
43	90,405.339(9)	92,391.10(2)	
44	90,566.527(9)	92,549.98(2)	
45	90,731.296(9)	92,712.33(2)	
46	90,899.610(9)	92,878.20(3)	
47	91,071.50(1)	93,047.54(3)	
48	91,246.90(2)	93,220.41(4)	
49	91,425.85(2)		
50			

[a] In cm^{-1}.
[b] Obtained in the final deperturbation analysis using a least-squares fitting procedure for the simultaneous determination of the molecular constants and term values (described in details in Refs. [71–74]) and PGOPHER software modified according to this purpose [50]. The uncertainties in parentheses indicate the random (fitting) errors of the terms.

A matrix of parameter correlations was consulted at various stages during the model fitting to determine which are independently relevant and ensure the final selection of parameters has a low degree of mutual correlation. The root-mean-square error of model line frequencies in the final fit is 0.01 cm^{-1} and demonstrates that the comprehensive perturbation model reproduces the experimental data very well. This value is also consistent with the average measurement accuracy. Experimental term values of $A^1\Pi(v = 1)$, $a'^3\Sigma^+(v = 10)$, $D^1\Delta(v = 1)$, and $I^1\Sigma^-(v = 2)$ are derived and reported in Table 13 and plotted in reduced form versus $J(J+1)$ in Fig. 7.

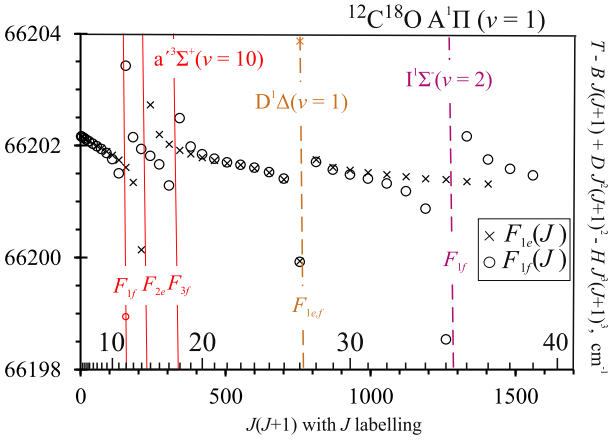

Fig. 7. Reduced ro-vibronic terms of the $^{12}C^{18}O$ $A^1\Pi(v = 1)$ level and its perturbers in the observed region. The presented A(1) terms were derived on the basis of the experimental data obtained in this work. The perturber terms were plotted on the basis of observed extra lines (solid lines) as well as on theoretical values calculated using isotopic rescaling of the molecular parameters given in the literature (see Table 11 for details).

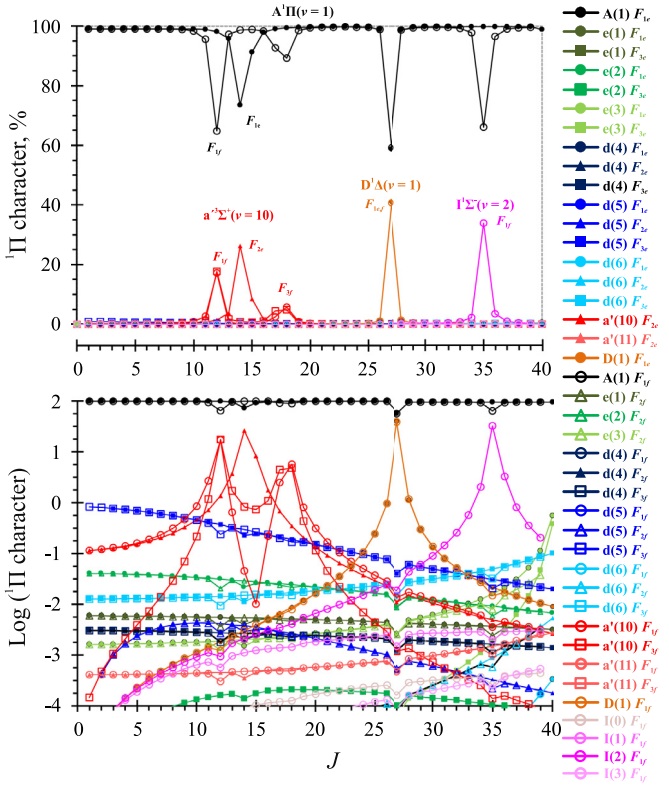

Fig. 8. Percentage $A^1\Pi$ character of the levels, which have meaningful influence on $A^1\Pi(v = 1)$ in $^{12}C^{18}O$. The lower figure presents logarithm of the character. See also Table 10 for details.

The modelled intra-molecular interaction of each perturber state ro-vibrational e- and f-symmetry level with $A^1\Pi(v = 1)$ may be expressed by its admixture of $A^1\Pi$ character as a percentage $C_{ik}^2 \cdot 100\%$ where $C_{ik} = \langle \Phi_k | \Psi_i \rangle$ is the mixing coefficient extracted from the model eigenvectors of the diagonalised energy matrix in our final model. The mixing percentages are presented in Fig. 8 and on a logarithmic scale to highlight the influence of states that perturb A(1) only weakly.

Table 13
Term values of the $A^1\Pi(v = 1)$ level and its perturbers in $^{12}C^{18}O$.[a,b]

J	$A^1\Pi(v = 1)$		$D^1\Delta(v = 1)$		$a'^3\Sigma^+(v = 10)$			$I^1\Sigma^-(v = 2)$
	F_{1e}	F_{1f}	F_{1e}	F_{1f}	F_{1f}	F_{2e}	F_{3f}	F_{1f}
1	66,205.133(1)	66,205.135(1)						
2	66,211.151(1)	66,211.150(1)						
3	66,220.170(1)	66,220.168(1)						
4	66,232.198(1)	66,232.195(1)						
5	66,247.230(1)	66,247.227(1)						
6	66,265.269(1)	66,265.263(1)						
7	66,286.309(1)	66,286.302(1)						
8	66,310.355(1)	66,310.341(1)						
9	66,337.402(1)	66,337.371(1)						
10	66,367.443(1)	66,367.371(1)						
11	66,400.467(1)	66,400.231(1)			66,411.36(3)			
12	66,436.451(1)	66,438.264(1)			66,433.816(7)			
13	66,475.299(1)	66,476.105(1)						
14	66,516.209(1)	66,518.009(1)				66,522.804(5)		
15	66,563.906(1)	66,562.992(1)				66,553.51(3)		
16	66,611.485(1)	66,610.948(1)				66,589.511(9)		
17	66,662.401(1)	66,661.664(1)					66,669.53(2)	
18	66,716.379(2)	66,716.951(2)					66,710.438(9)	
19	66,773.378(3)	66,773.507(3)						
20	66,833.362(4)	66,833.427(4)						
21	66,896.344(6)	66,896.370(6)						
22	66,962.30(1)	66,962.314(7)						
23	67,031.25(1)	67,031.25(1)						
24	67,103.13(2)	67,103.14(2)						
25	67,178.007(6)	67,177.98(2)						
26	67,255.757(6)	67,255.73(4)						
27	67,335.128(8)	67,335.113(8)	67,339.05(1)	67,339.03(1)				
28	67,420.717(6)	67,420.674(8)						
29	67,507.308(6)	67,507.255(8)						
30	67,596.920(6)	67,596.846(8)						
31	67,689.487(7)	67,689.38(1)						
32	67,784.991(8)	67,784.831(9)						
33	67,883.42(2)	67,883.160(9)						
34	67,984.776(9)	67,984.24(2)						
35	68,089.06(2)	68,086.20(2)						68,094.75(3)
36	68,196.24(2)	68,197.04(2)						
37	68,306.31(2)	68,306.74(2)						
38		68,419.59(2)						
39		68,535.40(2)						

[a] In cm^{-1}. The uncertainties in parentheses indicate the random (fitting) errors of the terms. The calibration error is 0.007 cm^{-1}.
[b] Merged on the basis of: the $^{12}C^{18}O$ A – X(1, 0), B – A(0, 1), B – A (1, 1), and C – A(0, 1) bands as well as B(0), B(1), C(0) term values obtained in this work.

4. Discussion

The *a priori* identification of all states that could possibly perturb the $A^1\Pi(v = 1)$ level for rotational states up to $J = 50$ was made with the aid of Fig. 6. Consideration was made not only for levels exhibiting an anti-crossing with A(1) but also non-crossing states in the energetic vicinity. Following the final deperturbation analysis, the strongest interactions affecting A(1) are found to involve the $a'^3\Sigma^+(v = 10)$, $D^1\Delta(v = 1)$ and $I^1\Sigma^-(v = 2)$ levels, all of which exhibit a marked anti-crossing with A(1). The onset of an anti-crossing with the $e^3\Sigma^-(v = 3)$ level is revealed at high *J*. The interaction with $d^3\Delta(v = 5)$ occurs most intensively close to the band origin and then smoothly disappears toward higher *J*-levels. The d(6) and a(11) levels also exhibit an anti-crossing with A(1), but for very high *J* beyond our experimental range, thus for these cases, flotation of the interaction parameters during the least-squares fit is statistically unjustified. The A(1) level energies are also significantly influenced by the non-crossing levels I(0, 1, 3), e(1, 2), and d(4, 5). Among them, only the interactions parameters associated with I(1) and d(5) could be reliably floated in our final deperturbation analysis, in accordance with their sufficiently-small energetic separation from A(1) and sufficiently-large Franck-Condon overlap with it. No significant direct interaction of A(1) with the non-crossing $a^3\Pi(v = 11, 12)$ levels in its immediate vicinity is apparent in our data. The non-impact of A(1) ~ a(11, 12) interactions is due to negligibly-small vibrational overlap integrals: $\langle v_{A(1)}|v_{a(11)}\rangle = 2 \times 10^{-5}$, $\langle v_{A(1)}|v_{a(12)}\rangle = 6.1 \times 10^{-5}$. Also, no indirect influence on A(1) was found from possible interactions of the a(11, 12) levels with other perturbing states that are themselves coupled to A(1). All of the direct and indirect interactions that are tested involving the A(1) level are listed in Table 10 and the results of the fit are given in Table 11.

Electric dipole and spin-conservation selection rules forbid transitions to any of the aforementioned states interacting with $A^1\Pi(v = 1)$. Such transitions nevertheless derive some oscillator strength from their interactions. There are 21 extra lines observed in the present study, listed in Tables 4 and 9, and the spin-orbit interaction $A^1\Pi(v = 1) \sim a'^3\Sigma^+(v = 10)$ leads to spin-forbidden $B^1\Sigma^+(v = 0, 1) - a'^3\Sigma^+(v = 10)$, $C^1\Sigma^+(v = 0) - a'^3\Sigma^+(v = 10)$ and $a'^3\Sigma^+(v = 10) - X^1\Sigma^+(v = 0)$ transitions. Similarly, the $A^1\Pi(v = 1) \sim D^1\Delta(v = 1)$ ***L***-uncoupling interaction leads to observation of the $B^1\Sigma^+(v = 0, 1) - D^1\Delta(v = 1)$ and $C^1\Sigma^+(v = 0) - D^1\Delta(v = 1)$ transitions, which are prohibited by the $\Delta\Lambda = 0, \pm1$ selection rule of electric-dipole transitions. The $A^1\Pi(v = 1) \sim I^1\Sigma^-(v = 2)$ ***L***-uncoupling interaction leads to the observation of lines of $B^1\Sigma^+(v = 0) - I^1\Sigma^-(v = 2)$ even though transitions between Σ^+ and Σ^-states are also forbidden.

A dilution of the $^1\Pi$ character of the observed $A^1\Pi(v = 1)$ level is caused by its interaction with perturbing states in its vicinity and the percentage-mixing of $^1\Pi$ character into these is presented

in Fig. 8. The largest mixing occurs for the $D^1\Delta(v=1)$ level (41% $^1\Pi$ admixture for both F_{1e} and F_{1f} levels at $J=27$), the F_{1f} component of $I^1\Sigma^-(v=2)$ (34% at $J=35$) as well as the F_{2e} component of $a'^3\Sigma^+(v=10)$ (26% at $J=14$). Smaller admixtures occur for the F_{1f} and F_{3f} components of the $a'^3\Sigma^+(v=10)$ level (~18% at $J=12$ and ~5% for $J=17$ to 18, respectively) and for all components of the $d^3\Delta(v=5)$ level (~1% for $J=1$ to 3). The $^1\Pi$ character of $A^1\Pi(v=1)$ is commensurately decreased as a result of this state-mixing. As shown in Fig. 8, the $A^1\Pi(v=1)$ and $d^3\Delta(v=5)$ levels that do not exhibit an anti-crossing are most strongly mixed at low J, while their interaction gradually decreases toward higher rotational levels.

Many B – A(1, 1) and C – A(0, 1) lines are weak and/or blended: 45% in C – A(0, 1), 41% in B – A(1, 1) and 36% in B – A(0, 1); and have relatively uncertain frequencies. Their influence on the deperturbation analysis was then tested. Simulations neglecting all blended and weak lines of the aforementioned bands were performed and resulted in standard deviations of molecular constants, perturbation parameters, and terms as well as the overall RMS error that are worse than in the primary deperturbation analysis. This confirms that our model of these singlet states is very "soft" and every line, whether blended or weak, is significant.

The term values of $A^1\Pi(v=1)$ ro-vibrational levels and its perturbers are extracted from the experimental frequencies by the addition of ground state rotational energies, and are plotted in a reduced form in Fig. 7 that highlights local perturrelbations.The largest term energy shift (approx. 2.8 cm^{-1}) occurs for the rotation-electronic (***L***-uncoupling) interaction between A(1) ~ I (2) at $J=35$. This occurs despite: (*i*) the vibrational overlap integral $\langle \upsilon_{A(1)}|\widehat{\mathbf{B}(\mathbf{R})}|\upsilon_{I(2)}\rangle$ = -0.4588 cm^{-1} having a smaller magnitude than between A(1) and D(1)($\langle \upsilon_{A(1)}|\widehat{\mathbf{B}(\mathbf{R})}|\upsilon_{D(1)}\rangle$ = -0.5706 cm^{-1}); (*ii*) the distance between A(1) and I(2) levels at $J=35$ being larger (approximately 2.9 cm^{-1}) than the corresponding distance between A(1) and D(1) at $J=27$ (approximately 0.9 cm^{-1}). This is a result of a quadratic J-dependence of the heterogeneous A(1) ~ D(1) and A(1) ~ I(2) interactions. Also, the maximum energy-level perturbation of A(1) due to its spin-orbit interaction with $a'^3\Sigma^+(v=10)$ is 2 cm^{-1} and occurs at $J=12$. This is smaller than the maximum shift due to I(2), despite the near-degeneracy of the A(1) and a(10) J ==12 levels, separated by 2.8 cm^{-1}, because their vibrational-overlap integral, −0.1388, is less than for A(1) and I(2).

The deperturbed molecular constants of $A^1\Pi(v=1)$, $a'^3\Sigma^+(v=10)$, $D^1\Delta(v=1)$, and $I^1\Sigma^-(v=2)$ and their intramolecular interaction parameters are collected in Table 11. The resulting fitted values were obtained from a Hamiltonian expressed in terms of the rotational operator $\hat{\boldsymbol{N}}$ for total angular momentum excluding spin, in accordance with IUPAC recommendations [75]. When comparing our results with those presented in Refs. [26,28], it should be remembered that the latter are calculated with a Hamiltonian in terms of $\hat{\boldsymbol{R}}$, the operator for rotational angular momentum of the nuclear framework. The difference when switching from $\hat{\boldsymbol{R}}$ to $\hat{\boldsymbol{N}}$ operators relates mainly to an energy-level (T_v) shift of $B\Lambda^2$, and rotational constant (B) change of $2D\Lambda^2$ [51,76].

Some of the molecular parameter uncertainties in Table 11 are presented with more than two-digits after consideration of a measure of the overall sensitivity of the least-squares fit to these parameters, as defined by Watson [77]. The sensitivity S_j is defined as a change in a parameter value that increases the overall error of the fit by a factor by no more than $0.1/n_{par}$, where n_{par} is the number of the floated parameters and provides a useful guide as to how many digits should be quoted for the parameter to ensure that calculations can be reproduced. The number of parameter digits generated by the PGOPHER program used here are based on the S_j sensitivity but, if necessary, increased to 10 times the least-squares estimated standard error. Alternatively, reference [78] describes a sequential rounding and refitting procedure aimed at avoiding the publication of parameters to non-physical precision [51].

Small irregularities in the level energy progressions of $^{12}C^{18}O$ $B^1\Sigma^+(v=0,\ 1)$ and $C^1\Sigma^+(v=0)$ levels are presented in Fig. 5. The deviations of particular J levels are evident in our results and indicate local interactions near $J=12$ and 34 for B($v=0$), and $J=6$ for B($v=1$) with multiple unobserved states. These perturbations do not correlate well with the term value deviations found by Lemaire et al. [32]. We attribute this to the noise level of [32] being somewhat greater than the magnitude of energy perturbations. The confirmation of additional smaller deviations possibly occurring for B(0), B(1) and C(0) and the identification of the perturbing states responsible await a comparison with similar known effects in other isotopologues: $^{13}C^{18}O$ [45], $^{12}C^{18}O$ [22], $^{13}C^{17}O$ [49], $^{12}C^{16}O$ and $^{14}C^{16}O$ [70], and $^{13}C^{16}O$ [19]. The remeasurement of B – X and C – X bands made here is evidently necessary to observe the weak perturbations present.

5. Conclusion

Using complementary Fourier-transform spectroscopy techniques in the visible and vacuum-ultraviolet, a data set of 6 bands of the $^{12}C^{18}O$ isotopologue were obtained, specifically, $B^1\Sigma^+$ – $A^1\Pi(0,\ 1)$, (1, 1) and $C^1\Sigma^+$ – $A^1\Pi(0,\ 1)$ in emission and $A^1\Pi$ – $X^1\Sigma^+(1,\ 0)$, $B^1\Sigma^+$ – $X^1\Sigma^+(0,\ 0)$, (1, 0), and $C^1\Sigma^+$ – $X^1\Sigma^+(0,\ 0)$ in absorption. In total, 626 transitions including 21 extra-lines were included in a deperturbation analysis of the $^{12}C^{18}O$ $A^1\Pi(v=1)$ level. As a result, 157 deperturbed parameters were obtained, including: molecular constants and term values for A(1), a(10), D(1), I(2); the spin-orbit and rotation-electronic (***L***-uncoupling) interaction parameters mixing A(1) and its perturbers; and term values for B(0), B(1), and C(0). These term values and fitted parameters are significantly more accurate than in previous analyses of this isotopologue. In conclusion, the deperturbation of the $A^1\Pi(v==1)$ state of $^{12}C^{18}O$ contributes to unravelling the complex series of perturbations affecting this benchmark diatomic molecule.

Declaration of Competing Interest

The authors declare that they have no known competing financial interests or personal relationships that could have appeared to influence the work reported in this paper.

CRediT authorship contribution statement

M.I. Malicka: Investigation, Formal analysis, Data curation, Validation, Software, Writing - original draft, Writing - review & editing, Visualization. **S. Ryzner:** Visualization, Software, Formal analysis, Data curation. **A.N. Heays:** Investigation, Methodology, Software, Validation, Data curation, Formal analysis, Writing - original draft, Writing - review & editing, Visualization, Funding acquisition. **N. de Oliveira:** Investigation, Methodology, Software, Validation, Writing - review & editing. **R.W. Field:** Conceptualization, Methodology, Validation, Resources, Writing - review & editing, Funding acquisition. **W. Ubachs:** Conceptualization, Investigation, Methodology, Validation, Writing - review & editing, Resources, Funding acquisition. **R. Hakalla:** Conceptualization, Supervision, Project administration, Methodology, Software, Investigation, Formal analysis, Data curation, Validation, Resources, Writing - original draft, Writing - review & editing, Visualization, Funding acquisition.

Acknowledgments

RH thanks LASERLAB-EUROPE for support of this research [grant numbers EUH2020-RIP-654148, EC's-SPF-284464] and European

Regional Development Fund and the Polish state budget within the framework of the Carpathian Regional Operational Programme [grant number RPPK.01.03.00-18-001/10] through the funding of the Center for Innovation and Transfer of Natural Sciences and Engineering Knowledge of the University of Rzeszów. WU and AH thank the Dutch Astrochemistry Network (NWO) for support [grant number 648.000.021]. AH was funded by the NASA Postdoctoral Program through the NASA Astrobiology Institute. RWF is grateful to the US National Science Foundation [grant number CHE-1800410]. The authors are grateful to the general and technical staff of SOLEIL synchrotron for providing beam time under project numbers 20120653 and 20160118.

References

[1] Visser R, van Dishoeck EF, Black JH. The photodissociation and chemistry of CO isotopologues: applications to interstellar clouds and circumstellar disks. Astronomy & Astrophysics 2009;503:323–43 323-U56. doi:10.1051/0004-6361/200912129.
[2] Lyons JR, Young ED. CO self-shielding as the origin of oxygen isotope anomalies in the early solar nebula. Nature 2005;435:317–20. doi:10.1038/nature03557.
[3] Dame T, Hartmann D, Thaddeus P. The milky way in molecular clouds: A new complete CO survey. Astrophys J 2001;547:792–813. doi:10.1086/318388.
[4] Catling DC. Planetary atmospheres. Treatise on geophysics, 10. 2nd edn. Oxford: Elsevier; 2015.
[5] Konopacky QM, Barman TS, Macintosh BA, Marois C. Detection of Carbon Monoxide and Water Absorption Lines in an Exoplanet Atmosphere. Science 2013;339:1398–401. doi:10.1126/science.1232003.
[6] Noterdaeme P, Krogager J-K, Balashev S, Ge J, Gupta N, Kruehler T, et al. Discovery of a Perseus-like cloud in the early Universe H_1-to- H_2 transition, carbon monoxide and small dust grains at $z_{abs} \approx 2.53$ towards the quasar J0000+0048. Astronomy & Astrophysics 2017;597:A82. doi:10.1051/0004-6361/201629173.
[7] Dapra M, Niu ML, Salumbides EJ, Murphy MT, Ubachs W. Constraint on a cosmological variation in the proton-to-electron mass ratio from electronic CO absorption. Astrophys J 2016;826:192. doi:10.3847/0004-637X/826/2/192.
[8] Bally J, Langer WD. Isotope-selective photodestruction of carbon monoxide. Astrophys J 1982;255:143–8. doi:10.1086/159812.
[9] Glassgold A, Huggins P, Langer W. Shielding of CO from dissociating radiation in interstellar clouds. Astrophys J 1985;290:615–26. doi:10.1086/163019.
[10] Bennett CJ, Jamieson CS, Kaiser RI. Mechanistical studies on the formation and destruction of carbon monoxide (CO), carbon dioxide (CO_2), and carbon trioxide (CO_3) in interstellar ice analog samples. Phys Chem Chem Phys 2010;12:4032–55. doi:10.1039/b917162b.
[11] Sheffer Y, Lambert DL, Federman SR. Ultraviolet detection of interstellar $^{12}C^{17}O$ and the CO isotopomeric ratios toward X Persei. Astrophys J 2002;574:L171–4. doi:10.1086/342501.
[12] Bensch F, Pak I, Wouterloot JGA, Klapper G, Winnewisser G. Detection of $^{13}C^{17}O$ and observations of rare CO isotopomers toward the ρ Ophiuchi molecular cloud. Astrophys J Lett 2001;562:L185–8. doi:10.1086/338253.
[13] Smith RL, Pontoppidan KM, Young ED, Morris MR, van Dishoeck EF. High-precision $C^{17}O$, $C^{18}O$, and $C^{16}O$ measurements in young stellar objects: Analogues for CO self-shielding in the early solar system. Astrophys J 2009;701:163–75. doi:10.1088/0004-637X/701/1/163.
[14] Farrenq R, Guelachvili G, Sauval AJ, Grevesse N, Farmer CB. Improved Dunham coefficients for CO from infrared solar lines of high rotational excitation. J Mol Spectro 1991;149:375–90. doi:10.1016/0022-2852(91)90293-J.
[15] Krupenie PH. The band spectrum of carbon monoxide. vol. 5. National Standard Reference Data Series. Washington, DC: National Bureau of Standards; 1966.
[16] Tilford SG, Simmons JD. Atlas of the observed absorption spectrum of carbon monoxide between 1060 and 1900 Å. J Phys Chem Ref Data 1972;1:147–88. doi:10.1063/1.3253097.
[17] Eidelsberg M, Launay F, Ito K, Matsui T, Hinnen P, Reinhold E, et al. Rydberg-valence interactions of CO, and spectroscopic evidence characterizing the $C'^1\Sigma^+$ valence state. J Chem Phys 2004;121:292–308. doi:10.1063/1.1756579.
[18] Rytel M. Ångström system of the $^{12}C^{18}O$ molecule. Acta Physica Polonica A 1970;38:299–308.
[19] Janjić J, Danielak J, Kępa R, Rytel M. The Ångström bands of $^{13}C^{16}O$ and $^{12}C^{18}O$ molecules. Acta Physica Polonica A 1972;41:757–61.
[20] Kępa R. High-resolution emission-spectra of the 0-0, 0-1 and 0-2 bands of $E^1\Pi$ - $A^1\Pi$ and $B^1\Sigma^+$ - $A^1\Pi$ transitions in $^{12}C^{18}O$ molecule. Acta Physica Hungarica 1986;60:227–37. doi:10.1007/BF03156045.
[21] Kępa R, Ostrowska-Kopeć M, Piotrowska I, Zachwieja M, Hakalla R, Szajna W, et al. Ångström ($B^1\Sigma^+ \rightarrow A^1\Pi$) 0-1 and 1-1 bands in isotopic CO molecules: further investigations. J Phys B At Mol Opt Phys 2014;47:045101. doi:10.1088/0953-4075/47/4/045101.
[22] Trivikram TM, Hakalla R, Heays AN, Niu ML, Scheidegger S, Salumbides EJ, et al. Perturbations in the $A^1\Pi$, v = 0 state of $^{12}C^{18}O$ investigated via complementary spectroscopic techniques. Mol Phys 2017;115:3178–91. doi:10.1080/00268976.2017.1356477.
[23] Kępa R. Note on the Herzberg system of the isotopic CO molecules. Acta Physica Polonica 1969;A36:1109.
[24] Janjić J, Conkic L, Pesic D, Kępa R, Rytel M. Herzberg system of $^{12}C^{18}O$ molecule. J Mol Spectro 1978;72:297–300. doi:10.1016/0022-2852(78)90130-3.
[25] Kępa R, Rytel M, Rzeszut Z. The $E^1\Pi$ - $A^1\Pi$ system bands in $^{13}C^{16}O$ and $^{12}C^{18}O$ molecules. Acta Physica Polonica A 1978;54:355–61.
[26] Haridass C, Reddy S, Le Floch AC. The 4th Positive $A^1\Pi$ - $X^1\Sigma^+$ System of $^{12}C^{18}O$ and $^{13}C^{18}O$: Perturbations in the $A^1\Pi$ State. J Mol Spectro 1994;167:334–52. doi:10.1006/jmsp.1994.1240.
[27] Haridass C, Reddy SP, Le Floch AC. Precise Rovibronic Term Values of Some Vibrational Levels of the $A^1\Pi$, $B^1\Sigma^+$, $C^1\Sigma^+$, and $E^1\Pi$ States of $^{12}C^{18}O$ and $^{13}C^{18}O$. J Mol Spectro 1994;168:429–41. doi:10.1006/jmsp.1994.1291.
[28] Beaty LM, Braun VD, Huber KP, Le Floch AC. A high-resolution ^{18}C isotope study in the vacuum ultraviolet of the $A^1\Pi$ - $X^1\Sigma^+$ 4th positive system of CO. Astrophys J Suppl Series 1997;109:269–77. doi:10.1086/312976.
[29] du Plessis A, Rohwer EG, Steenkamp CM. Accurate laboratory wavelengths of the $A^1\Pi$(v'=0-5) -$X^1\Sigma^+$(v"=0) vibronic bands of $^{12}C^{17}O$ and $^{12}C^{18}O$. Astrophys J Suppl Series 2006;165:432–7. doi:10.1086/504428.
[30] Eidelsberg M, Roncin JY, Le Floch AC, Launayl F, Letzelter C, Rostas J. Reinvestigation of the vacuum ultraviolet-spectrum of CO and isotopic-species $B^1\Sigma^+ \leftrightarrow X^1\Sigma^+$ transition. J Mol Spectro 1987;121:309–36. doi:10.1016/0022-2852(87)90055-5.
[31] Stark G, Heays AN, Lyons JR, Smith PL, Eidelsberg M, Federman SR, et al. High-resolution oscillator strength measurements of the v = 0, 1 bands of the B-X, C-X, and E-X systems in five isotopologues of carbon monoxide. Astrophys J 2014;788:67–80. doi:10.1088/0004-637X/788/1/67.
[32] Lemaire JL, Heays AN, Eidelsberg M, Gavilan L, Stark G, Federman SR, et al. Atlas of new and revised high-resolution spectroscopy of six CO isotopologues in the 101-115nm range Transition energies of the v'=0, 1, 2, and 3 to v"=0 bands of the $B^1\Sigma^+$, $C^1\Sigma^+$, and $E^1\Pi$ to $X^1\Sigma^+$ states, related term values, and molecular constants. Astronomy & Astrophysics 2018;614:A114. doi:10.1051/0004-6361/201732114.
[33] Eidelsberg M, Rostas F. Spectroscopic, absorption and photodissociation data for CO and isotopic-species between 91 and 115 nm. Astronomy & Astrophysics 1990;235:472–89.
[34] Ubachs W, Hinnen P, Hansen P, Stolte S, Hogervorst W, Cacciani P. Laser spectroscopic studies of the $C^1\Sigma^+$, ($v = 0$) and ($v = 1$) states of CO. J Mol Spectro 1995;174:388–96. doi:10.1006/jmsp.1995.0010.
[35] Cacciani P, Brandi F, Velchev I, Lyngå C, Wahlström C-G, Ubachs W. Isotope dependent predissociation in the $C^1\Sigma^+$, v= 0 and v= 1 states of CO. Eur Phys J D 2001;15:47–56. doi:10.1007/s100530170182.
[36] Ubachs W, Velchev I, Cacciani P. Predissociation in the $E^1\Pi$, v=1 state of the six natural isotopomers of CO. J Chem Phys 2000;113:547–60. doi:10.1063/1.481830.
[37] Roncin JY, Ross A, Boursey E. The C→B(O-O) band of 4 isotopes of carbon-monoxide. J Mol Spectro 1993;162:353–7. doi:10.1006/jmsp.1993.1290.
[38] Field RW. Spectroscopy and perturbation analysis in excited states of CO and CS. PhD thesis. Harvard University; 1971.
[39] Field RW, Simmons JD, Tilford SG, Wicke BG. Analysis of perturbations in $a^3\Pi$ and $A^1\Pi$ states of CO. J Mol Spectro 1972;44:383–99. doi:10.1016/0022-2852(72)90111-7.
[40] Niu ML, Salumbides EJ, Zhao D, de Oliveira N, Joyeux D, Nahon L, et al. High resolution spectroscopy and perturbation analysis of the CO $A^1\Pi - X^1\Sigma^+$ (0,0) and (1,0) bands. Mol Phys 2013;111:2163–74. doi:10.1080/00268976.2013.793889.
[41] Niu ML, Salumbides EJ, Heays AN, de Oliveira N, Field RW, Ubachs W. Spectroscopy and perturbation analysis of the CO $A^1\Pi - X^1\Sigma^+$ (2,0), (3,0) and (4,0) bands. Mol Phys 2016;114:627–36. doi:10.1080/00268976.2015.1108472.
[42] Niu ML, Hakalla R, Trivikram TM, Heays AN, de Oliveira N, Salumbides EJ, et al. Spectroscopy and perturbation analysis of the $A^1\Pi$ (v=0) state of $^{13}C^{16}O$. Mol Phys 2016;114:2857–67. doi:10.1080/00268976.2016.1218078.
[43] Hakalla R, Niu ML, Field RW, Salumbides EJ, Heays AN, Stark G, et al. VIS and VUV spectroscopy of $^{12}C^{17}O$ and deperturbation analysis of the $A^1\Pi$, v = 1–5 levels. R Soc Chem Adv 2016;6:31588–606. doi:10.1039/C6RA01358A.
[44] Hakalla R, Niu ML, Field RW, Heays AN, Salumbides EJ, Stark G, et al. Fourier-transform spectroscopy of $^{13}C^{17}O$ and deperturbation analysis of the $A^1\Pi$ (υ=0–3) levels. J Quant Spectro Rad Transf 2017;189:312–28. doi:10.1016/j.jqsrt.2016.12.012.
[45] Hakalla R, Trivikram TM, Heays AN, Salumbides EJ, de Oliveira N, Field RW, et al. Precision spectroscopy and comprehensive analysis of perturbations in the $A^1\Pi$(v = 0) state of $^{13}C^{18}O$. Mol Phys 2019;117:79–96. doi:10.1080/00268976.2018.1495848.
[46] Hakalla R. First analysis of the Herzberg ($C^1\Sigma^+ \rightarrow A^1\Pi$) band system in the less-abundant $^{13}C^{17}O$ isotopologue. R Soc Chem Adv 2014;4:44394–407. doi:10.1039/C4RA08222B.
[47] Hakalla R, Zachwieja M, Szajna W. First analysis of the $B^1\Sigma^+$(v = 1) Rydberg state in the lesser-abundant $^{12}C^{17}O$ isotopologue on the basis of the 1–v″ progression of the Ångström band system. J Quant Spectro Rad Transf 2014;140:7–17. doi:10.1016/j.jqsrt.2014.02.004.
[48] Hakalla R. Investigation of the Herzberg ($C^1\Sigma^+ \rightarrow A^1\Pi$) band system in $^{12}C^{17}O$. J Quant Spectro Rad Transf 2015;164:231–47. doi:10.1016/j.jqsrt.2015.06.016.
[49] Hakalla R, Niu ML, Field RW, Heays AN, Salumbides EJ, Stark G, et al. Fourier-transform spectroscopy of $^{13}C^{17}O$ and deperturbation analysis of the $A^1\Pi$ (v=0–3) levels. J Quant Spectro Rad Transf 2017;189:312–28. doi:10.1016/j.jqsrt.2016.12.012.

[50] Western C. PGOPHER: a program for simulating rotational structure. Development version. Bristol: University of Bristol; 2020 http://Pgopher.Chm.Bris.Ac.Uk/.
[51] Western C. PGOPHER: A program for simulating rotational, vibrational and electronic spectra. J Quant Spectro Rad Transf 2017;186:221–42. doi:10.1016/j.jqsrt.2016.04.010.
[52] De Oliveira N, Joyeux D, Roudjane M, Gil J-F, Pilette B, Archer L, et al. The high-resolution absorption spectroscopy branch on the VUV beamline DESIRS at SOLEIL. J Synchrotron Rad 2016;23:887–900. doi:10.1107/S1600577516006135.
[53] Nahon L, de Oliveira N, Garcia GA, Gil J-F, Pilette B, Marcouille O, et al. DESIRS: a state-of-the-art VUV beamline featuring high resolution and variable polarization for spectroscopy and dichroism at SOLEIL. J Synchrotron Rad 2012;19:508–20. doi:10.1107/S0909049512010588.
[54] Niu ML, Ramirez F, Salumbides EJ, Ubachs W. High-precision laser spectroscopy of the CO $A^1\Pi$ - $X^1\Sigma^+$ (2,0), (3,0), and (4,0) bands. J Chem Phys 2015;142:044302. doi:10.1063/1.4906244.
[55] Niu ML, Heays AN, Jones S, Salumbides EJ, van Dishoeck EF, De Oliveira N, et al. VUV-synchrotron absorption studies of N_2 and CO at 900 K. J Mol Spectro 2015;315:137–46. doi:10.1016/j.jms.2015.02.011.
[56] Dreissen LS, Roth C, Grundeman EL, Krauth JJ, Favier M, Eikema KSE. High-Precision Ramsey-Comb Spectroscopy Based on High-Harmonic Generation. Phys Rev Lett 2019;123:143001. doi:10.1103/PhysRevLett.123.143001.
[57] Brandi F, Velchev I, Hogervorst W, Ubachs W. Vacuum-ultraviolet spectroscopy of Xe: Hyperfine splittings, isotope shifts, and isotope-dependent ionization energies. Phys Rev A 2001;64:032505. doi:10.1103/PhysRevA.64.032505.
[58] Drabbels M, Heinze J, Termeulen J, Meerts W. High-resolution double-resonance spectroscopy on Rydberg states of CO. J Chem Phys 1993;99:5701–11. doi:10.1063/1.465919.
[59] Coxon JA, Hajigeorgiou PG. Direct potential fit analysis of the $X^1\Sigma^+$ ground state of CO. J Chem Phys 2004;121:2992–3008. doi:10.1063/1.1768167.
[60] Lefebvre-Brion H, Field RW. The spectra and dynamics of diatomic molecules. Amsterdam: The Netherlands: Elsevier Academic Press; 2004.
[61] Le Floch AC, Launay F, Rostas J, Field RW, Brown CM, Yoshino K. Reinvestigation of the CO $A^1\Pi$ state and its perturbations – the v=0 levels. J Mol Spectro 1987;121:337–79. doi:10.1016/0022-2852(87)90056-7.
[62] Le Floch AC, Rostas J, Schamps J. The $A^1\Pi \sim D\ ^1\Delta$ rotation-electronic interaction in CO. Mol Phys 1988;63:677–84. doi:10.1080/00268978800100481.
[63] Tilford SG, Howard RA, Ginter ML. Fluorescence of carbon-monoxide excited by 1306-Å oxygen resonance line. J Chem Phys 1972;56:1413–15. doi:10.1063/1.1677380.
[64] Kittrell C, Garetz BA. Analysis of the $D^1\Delta$ - $X^1\Sigma^+$ transition in CO observed by two-photon excitation. Spectrochim Acta 1989;45:31–40. doi:10.1016/0584-8539(89)80024-8.
[65] Wolk G, Rich J. Observation of a new electronic state of carbon-monoxide using LIF on highly vibrationally excited CO ($X^1\Sigma^+$). J Chem Phys 1983;79:12–18. doi:10.1063/1.445571.
[66] Vázquez GJ, Amero JM, Liebermann HP, Lefebvre-Brion H. Potential Energy Curves for the $^1\Sigma^+$ and $^{1,3}\Pi$ States of CO. J Phys Chem A 2009;113:13395–401. doi:10.1021/jp902730d.
[67] Kępa R. New spectroscopic studies of the Herzberg bands of the $^{12}C^{16}O$ molecule. J Mol Spectro 1989;135:119–30. doi:10.1016/0022-2852(89)90359-7.
[68] Huber KP, Herzberg G. Constants of diatomic molecules. New York: Nostrand Reinhold; 1979.
[69] Rytel T. Analysis of the Perturbed 2-2 Band of the Third Positive ($b^3\Sigma^+$- $a^3\Pi_r$) System of CO. J Mol Spectro 1992;151:271–4.
[70] Amiot C, Roncin JY, Verges J. First observation of the CO $E^1\Pi$ to $B^1\Sigma^+$ and $C^1\Sigma^+$ to $B^1\Sigma^+$ band systems. Predissociation in the $E^1\Pi$(v=0) level. J Phys B Atom Mol Phys 1986;19:L19–23. doi:10.1088/0022-3700/19/1/004.
[71] Åslund N. Numerical-method for simultaneous determination of term values and molecular-constants. J Mol Spectros 1974;50:424–34. doi:10.1016/0022-2852(74)90245-8.
[72] Curl R, Dane C. Unbiased least-squares fitting of lower states. J Mol Spectro 1988;128:406–12. doi:10.1016/0022-2852(88)90157-9.
[73] Watson J. On the use of term values in the least-squares fitting of spectra. J Mol Spectro 1989;138:302–8. doi:10.1016/0022-2852(89)90119-7.
[74] Focsa C, Poclet A, Pinchemel B, Le Roy R, Bernath P. Fourier transform spectroscopy of the $A'^1\Pi$ - $X^1\Sigma^+$ system of CaO. J Mol Spectro 2000;203:330–8. doi:10.1006/jmsp.2000.8187.
[75] Hirota E, Brown J, Hougen J, Shida T, Hirota N. Symbols for fine and hyperfine-structure parameters. Pure Appl Chem 1994;66:571–6. doi:10.1351/pac199466030571.
[76] Brown JM, Howard BJ. An approach to the anomalous commutation relations of rotational angular momenta in molecules. Mol Phys 1976;31:1517–25. doi:10.1080/00268977600101191.
[77] Watson JKG. Rounding errors in the reporting of least-squares parameters. J Mol Spectro 1977;66:500–2. doi:10.1016/0022-2852(77)90308-3.
[78] Le Roy RJ. Uncertainty, Sensitivity, Convergence, and Rounding in Performing and Reporting Least-Squares Fits. J Mol Spectro 1998;191:223–31. doi:10.1006/jmsp.1998.7646.